Jimma University
School of Graduate Studies
Jimma Institute of Technology

Faculty of Electrical and Computer Engineering

M.Sc. In Electronics Communication Engineering

Performance Enhancement of Metamaterial Inspired Millimeter-Wave Antenna Arrays for 5G Wireless Applications

A Thesis Submitted to Jimma Institute of Technology, School of Graduate Studies in Partial Fulfillment of the Requirements for Masters Degree in Communication Engineering.

By:

Moti Beyene Gole

April 13, 2024

Jimma, Ethiopia

Declaration

I, hereby declare that the thesis titled "**Performance Enhancement of Metamaterial Inspired Millimeter-Wave Antenna Arrays for 5G Wireless Applications**" is entirely my original work. I affirm that this thesis has not been submitted for any other academic qualification, and all sources used are properly acknowledged. I further declare that no part of this thesis has been previously published or submitted for any degree or diploma.

A thesis submitted by

Moti Beyene Gole 14/04/2024

Signature Date

APPROVED BY BOARD OF EXAMINERS.

1. **Dr. Mohammed Muntaz** 26/04/2024
   Chairman Dept. of
   Graduate Committee

   Signature Date

2. **Dr. Isayiyas Nigatu** 26/04/2024
   Advisor

   Signature Date

3. **Dr. Kinde Anley** *15/04/2024*
   Internal Examiner

   Signature Date

4. **Dr. Bekele Mulu** 15/4/2024
   External Examiner

   Signature Date

April 13, 2024
Jimma, Ethiopia

Abstract

Fifth-generation (5G) wireless communication systems employ millimeter-wave (mm-wave) frequency bands to achieve a very broad spectrum for high data rate transmission. To meet the requirements of the system, the design of antenna arrays with high capacitance and flexibility are essential. Thus, in this thesis, the design and performance analysis of single element, 2x1, 4x1, 2x2, 4x4, and 8x8 metamaterial inspired millimeter wave antenna (MIA) arrays are proposed. Rogers' 5880, a substrate material with a 2.2 dielectric constant and a thickness of 0.35 mm, is used in the design of the antenna elements to operate at a 38 GHz central frequency. The simulated design of the single, 2x1, 4x1, 2x2, 4x4, and 8x8 MIA arrays bandwidth and total efficiencies ($\eta\%$) are: 1.971 GHz, 2.278 GHz, 4.704 GHz, 2.51 GHz, 4.156 GHz, 5.44 GHz; and 95.55 %, 94.01 %, 95.87%, 95.58%, 93.21%, and 85.38% respectively. As compared to other works, improved performance has been achieved by considering the effect of metamaterials on the radiator and at the ground of microstrip patch antennas (MPA). The selected type of metamaterials alters the current distribution of the radiating patch that enhances the fringing fields at the edge of MPAs, which inspires the radiation of antennas and reduces the surface wave loss at the radiators' ground plane. The proposed MIA antenna arrays have improved on the drawbacks of traditional MPAs in terms of bandwidth, VSWR, and return losses to enhance the data rate and device to device communication for 5G wireless systems.

keywords: Bandwidth, Beam-Gain, Directivity, Meta-material, Split Ring Resonator, and Return loss.

Acknowledgment

First, I express my gratitude to God for granting me the health, stamina, and perseverance necessary to complete this thesis. I appreciate the unwavering support, guidance, insights, and encouragement provided by my advisor, Dr. Isayiyas Nigatu as they played a pivotal role in helping me to conclude this study. I also express my thanks to the Jimma Institute of Technology for providing me with this opportunity. Special appreciation goes to the dedicated staff at the School of Electrical and Computer Engineering for their contributions to the success of this thesis. And finally, I want to sincerely thank my lovely wife Shume Asefa for her unwavering prayers and support.

Contents

List of Figures

List of Tables

Abbreviation and Acronyms

5G.....Fifth Generation

CRLH.....Composite Left and Right-Hand material

CST .....Computer Simulation Technology

CWG.....Co-planar Wave Guide

CSRR.....Complementary Split-ring resonator

CPW.....Coplanar waveguides

DPS.....Double Positive Material

DNG..... Double negative material

ENG.....Epsilon Negative Material

EBG.....Electromagnetic Band Bap

FSS.....Frequency Selective Surface

GPS.....Global Positioning System

HFSS.....High-Frequency Electromagnetic Simulation Software

LHM.....Left-Handed Materials

MIA.....Metamaterial-Inspired Antenna

MIMO.....Multiple Input-Multiple Output

MNG.....Mu Negative Material

MPA.....Microstrip patch antenna

PCB.....Printed Circuit Board

PBG.....Photonic Band gap

PMC.....Perfectly Magnetic Conductors

SRR.....Split Ring Resonator

SMT.....Surface Mount Technology

RIS.....Reactive Impedance Surface

UNII.....Unlicensed National Information Infrastructure

UWB.....Ultra Wide Band

UNII.....Unlicensed National Information Infrastructure

VSWR.....Voltage Standing Wave Ratio

Chapter 1

1 Introduction

1.1 Background of the Study

The advent of fifth generation (5G) in wireless innovation is fundamentally transforming telecommunications. The growth of wireless data applications and the increasing prevalence of smart devices have resulted in a significant expansion of wireless data traffic [1, 4]. This expansion presents both challenges and prospects for mobile service providers, prompting them to navigate the complexities of increased demand while simultaneously exploring opportunities for innovation and improved service delivery[1]. 5G is projected to enable more economic growth through the digitization of a connected society, encompassing people and all possible items, and the readiness for the growth of smart cities, smart agriculture, smart grids, energy, smart manufacturing, autonomous driving, logistics, public safety, and numerous other verticals[4]. The network requirements are on the rise due to the anticipated enormous development in associated devices and a significant increase in information activity shortly [4]. However, the overwhelming challenge to reaching these heights, as has continuously been the case with mobile communications, is the availability of valuable and applicable spectrum [1].

5G systems are deployed in various spectrum bands; such as below 1 GHz, between 1 and 6 GHz, and, for the first time in the spectrum beyond 6 GHz in the mm-wave frequency range. The utilization of the underutilized mm-wave bands (officially 30 to 300 GHz), particularly referring to the 24 GHz spectrum, is responsible for the bandwidth scarcity that occurs in wireless applications[2]. These frequencies offer a large amount of spectrum, with approximately 100 GHz defined for 5G broadband mobile communication networks. The range of millimeter waves, combined with the low-, mid-band spectrum, and the novel technologies to fully leverage the 30-300GHz spectrum, are expected to significantly boost the performance of 5G cellular networks with increased spectrum bandwidth, massive parallel communications, and ultra-dense networks. 5G,

the latest radio technology, is the first mobile technology generation to make use of the mm-wave spectrum [1].

As the mobile communications industry continues to make strides in the development and deployment of 5G systems in the mm-wave band, a wealth of new information has emerged regarding methodologies, performance results, and insights gained from various trials and deployments, providing valuable insights into the mm-wave spectrum, its advantages and the difficulties in this field[2]. As 5G systems at millimeter wave frequencies progress, a notable example of anticipated outcomes is their ready applicability to provide enhanced mobile broadband services. This enables operators to meet the increased need for high-speed data among average users in outdoor deployment scenarios (e.g., dense urban micro, suburban, etc.)d[2]. 5G NR mm-Wave offers a compelling complement to existing communication deployments, both for indoor venues (e.g., convention centers, event halls, concerts, indoor stadiums, etc.) and in enterprise deployments (e.g., office buildings, shop floors, meeting rooms, auditoriums, etc.). Mm-Wave can provide new and enhanced experiences with multi-Gbps data rates, low latency, and virtually unlimited capacity, supporting various devices beyond smartphones, tablets, and laptops. It delivers on this promise through dense spatial reuse enabled by beam-forming at both the cell site and device, utilizing vast amounts of spectrum [2, 3].

However, deploying mobile communications in the mm-wave range, commonly referred to as the mm-wave spectrum, poses challenges due to the harsh radio frequency (RF) environment within the domain of frequencies in the higher spectrum range. Factors such as higher path loss, reduced scattering, a resulting decrease in channel diversity, and increased blockage from weaker non-line-of-sight paths need to be addressed for efficient mobile communications in the millimeter-wave spectrum [3]. Additionally, the impact of noise power is more pronounced in millimeter waves due to the usage of larger bandwidths. Several issues must be overcome to use this spectrum effectively. Massive MIMO, beamforming, and using small cells or ultra-cell densification are key solutions for 5G mobile developments in millimeter waves. Understanding and develop-

ing these technologies effectively can unlock exciting new horizons in mobile broadband communications [3].

The frequency bands range from low-band to mm-wave, with specific considerations for antennas supporting compact designs, especially in millimeter-wave frequencies like 28 GHz, where phased array configurations are prevalent [2]. Metamaterials offer a promising perspective by enabling miniaturization, improving gain, and tailoring bandwidth for specific 5G frequency bands. Various antenna components, must be carefully chosen to minimize signal loss and ensure high transmission efficiency [2]. The integration with diverse infrastructure, environmental resistance, durability, and cost-effectiveness are additional factors in the complex landscape of antenna material selection for 5G. The continuous exploration of innovative design approaches remains essential as 5G technology evolves and expands [2].

1.2 Millimeter Wave Spectrum

In the context of the 5G industry, spectrum usage extends to slightly longer wavelengths than mm-waves, including frequencies like 24 GHz, and 28 GHz which share many functional properties. Frequencies at 30 GHz and higher, are collectively termed millimeter waves [2]. The primary attraction of the microwave spectrum lies in its extensive bandwidth, which enables the delivery of gigabit wireless services. Another advantage is the diminutive size of antennas used for transmission and reception. This allows for packing several hundred antenna components into a small area, facilitating high antenna gains and beam formation, even in handsets. Advances in silicon manufacturing have significantly reduced the cost of mm-wave hardware, making it feasible for consumer electronics. Ongoing research and development further indicate the promising integration of mm-Wave into 5G systems [2].

The significant propagation attenuation in the millimeter-wave frequency band may provide additional benefits in terms of frequency reuse and communication security. Overcoming obstacles, such as radio channel measurement modeling and estimation,

antenna design and measurement, beamforming and energy efficiency, commercial hardware design and development, multi-cell cooperation, network planning, and interference, system performance assessment, and optimization, as well as the exploration of new use cases and 5G applications, is crucial for the commercial viability of 5G millimeter-wave communications [4].

However, millimeter waves face challenges related to limited range and susceptibility to atmospheric absorption and blockage by obstacles. Metamaterials, conversely, present a promising avenue for overcoming some of these challenges. They are crafted to display electromagnetic properties that are distinct and not naturally present in materials [4]. Metamaterials can be customized to interact with and control millimeter waves. This capability enables the design of compact antennas, beamforming structures, and devices that enhance signal propagation, mitigate absorption losses, and optimize performance across communication systems operating in the millimeter-wave range. The integration of metamaterials in the millimeter-wave spectrum holds the potential for advancing the capabilities and overcoming the limitations associated with these frequencies, contributing to the effective deployment of high-speed and low-latency wireless communication technologies [2].

1.3 Meta-materials

The word "meta-material" is the Greek words "meta" and "material," where "meta" denotes something above and beyond the ordinary, altered, transformed, or advanced [5]. It is an artificial substance made to have physical qualities that are not present in natural substances [5]. The term "metamaterial" was originated by Rodger M. Walser, who also defined the term: "Macroscopic-composite materials with artificial three-dimensional periodic cellular architecture intended to produce the flawless combination of two or more reactions that do not occur normally" [5, 6]. Numerous definitions of electromagnetic meta-materials are put out, all of which can help us comprehend this concept as follows:

- The creation of homogeneous metal structures yields electromagnetic metama-

terials, which are manmade materials with peculiar features not seen in natural materials [7].

- To create a unit cell of meta-materials, an effective homogeneous structure must be significantly less than the bounded wavelength[6].
- When micro-structures known as cells are placed, metamaterials are created.
- These cells can be constructed from dielectric, electrical, or non-electric materials [7].
- Atoms can be arranged in an organized or chaotic way, to achieve the necessary macro-characteristics for the metamaterial.
- Conversely, various structures yield distinct types of metamaterials, and their applications are categorized based on the material's permittivity and permeability values generated by these structures [7].

1.4 Unit cell of metamaterials

The metamaterials used in the antenna design can take the shape of an array made up of several unit cells. Therefore, the primary factors influencing the resonance frequency, permittivity, and permeability of its unit cell must be designed and analyzed as the initial stage in building the antenna metamaterials[8]. The unit cell design for metamaterials is derived by calculating sizes and simulating unit cells to ensure that the permittivity (ϵ) and permeability (μ) parameters meet the specified requirements at the anticipated resonant frequency. The unit cell array of the antenna design is the form of the metamaterials. As a result, the first step in creating antenna metamaterials is to create and evaluate the primary variables that influence the fundamental structural unit's resonance frequency, permittivity, and permeability. The design of unit cells of metamaterials is the modeling of unit cells and size computation, so that the parameters permittivity and permeability at the anticipated resonance frequency, these unit cells will meet the requirements. For each unit cell type, the dimensions of the unit cell can be adjusted to satisfy conditions at resonant frequency. Depending

on the arrangement of the metamaterial, a unit cell is typically less than 1/10 of the operational wavelength, although the size varies [9].

1.5 Statement of the Problem

There have been recent events of interest in the need to miniaturize and integrate several features into wireless communication devices, especially those that could be substantially used in conjunction with 5G applications. To fulfill this requirement,the 5G application materials ought to be compact, able to multi-function, and sufficient with bandwidth operation. Despite their widespread use in a variety of applications, conventional antennas have several material restrictions that need to be carefully taken into account when the design is being developed. The characteristics frequently limit antennas' performance; therefore, careful design technique and selection of metamaterials required to enhance the performance.

Aside from the requirement for compatibility and optimization, other factors to take into account are cost, availability, and integration with active components. Therefore, this study proposed to get around these restrictions and improve the performance of antennas in a variety of applications, investigating materials and design techniques. An antenna is certainly considered one among them; it ought to be consistent with the frame of the device, decreased in size, and successful in running at a high-performance level. Nowadays, there are numerous technical answers implemented inside antenna production to meet these requirements. Microstrip antenna technology is currently made more compact by using pins that are shorted to a wall and a substrate with a high permittivity. However, these techniques have shortcomings, large return loss, and minimal gain. Therefore, to mitigate this kind of disadvantage, it is necessary to improve the antenna design and method by using SRR meta-materials that will increase bandwidth, and antenna gains, as well as improve various antenna parameters with the reduction of antenna dimensions and the return loss.

1.6 Research Questions

To improve MIA arrays performance; the following questions will be answered at the end of the thesis.

- How to enhance bandwidth, gain, and radiation efficiency of metamaterial-inspired antenna arrays?
- How to minimize different losses in metamaterial-inspired antenna arrays?

1.7 Objectives

1.7.1 General Objective

The general objective of this thesis work is to enhance the performance of metamaterial-inspired mm-wave antenna arrays for 5G wireless applications.

1.7.2 Specific Objectives

The specific objectives of the study are:

- To enhance the performance of meta-material-inspired antenna arrays regarding bandwidth, radiation beam gain, and radiation efficiency for 5G wireless applications.
- To minimize surface wave and spurious wave losses in antenna arrays.
- To mitigate mutual coupling and impedance mismatch of antenna arrays.

1.8 System Design and Methodology

- **System design:** This involves determining different antenna parameters, and types of antenna simulation software. Analyzing various metamaterial inspired models used in the millimeter-wave for 5G wireless applications. To improve the performance of an antenna the following techniques have been used.
  - Designing meta-material unit cells and arrays.

  - Designing millimeter-wave meta-materials as an antenna to improve bandwidth, efficiency, and size of an antenna.
  - Designing millimeter wave meta-materials as the ground of an antenna for reducing the return loss and increasing antenna propagation.

- **Simulation:** To analyze the performance of metamaterial-inspired millimeter-wave antenna; unit cells and antenna parameters are designed and simulated using CST Studio Suite simulation.
- **Analysis of the simulation results.**
- **Conclusion and recommendations**

1.9 Scope of the Study

This thesis analyzes the performance of millimeter-wave MIA arrays for 5G wireless applications. Improving antenna parameters, mitigating mutual coupling, and reducing the size of antennas are the main concepts of this proposed work. The analysis of metamaterial antennas and the fringing properties of conventional and proposed works have been studied. The design procedure has been started by studying the properties of metamaterial unit cells, and merging with conventional antennas is the first step of the thesis. The single, 2x1, 4x1, 2x2, 4x4, and 8x8 MIAs are designed and simulated by their perspective steps. The simulated results of different MIA have been compared with different literature.

1.10 Significance of the Study

The benefit of this thesis will be the ability to use smooth communication, large data exchange, compact size of the device, and communication at large frequencies with low latency. For 5G applications, this thesis will help by using sufficient bandwidth, decreasing the power loss of the system and the volume fraction of antennas. Also high-speed communication for devices and fulfill the requirements for 5G applications by enhancing the performance of the model and familiarizing ourselves with high frequencies.

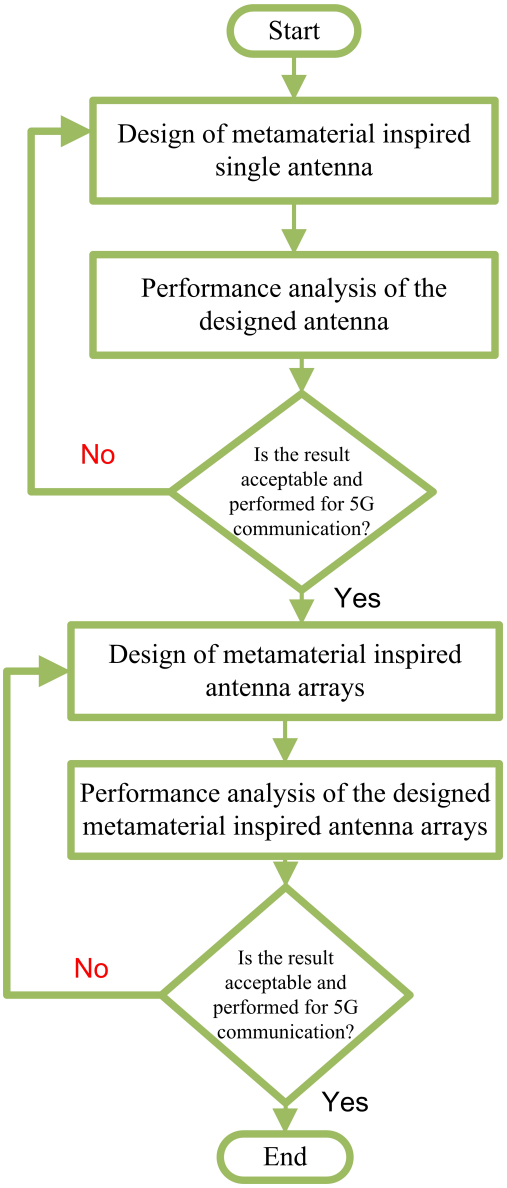

Figure 1.1: Block diagram of proposed methodology

1.11 Organization of the Thesis

The thesis is organized into six chapters. Chapter one includes an introduction of the thesis context, a clear statement of the problem, the thesis objectives, system design and methodology, research questions, anticipated outcomes of the investigation, scope of the research, and organization of the thesis. The second chapter has theoretical reviews and conceptual frameworks of different antennas that were designed and proposed by different authors at different times. The third chapter discussed fundamentals of antennas and metamaterials, with subsections on the fundamentals of antennas, meta-

materials, and antenna miniaturization based on metamaterials. Design of MIAs in the thesis has been discussed in chapter 4. The simulation result and discussion were analyzed under chapter 5. To conclude the thesis, chapter 6 has a conclusion and a future work that has been studied and analyzed in the thesis.

Chapter 2

2 Literature Review

In recent years, meta-materials have been a sensitive area for researchers to discuss how to increase antenna performance for 5G applications. In this chapter, different works and literatures based on MIAs reviewed and synthesized.

Due to the related number of multi-band frequencies and limited bandwidths [10], the consecutive resonant frequency will interfere with each other. The design [10] to make compact in size and operate at a single frequency band has limited. Antennas designed using left-handed material [11], present surveillance equipment with automated dependence receiver equipment. According to the result of the study using left-handed metamaterial has no values added to the performance of conventional microstrip antennas. The studied result in [11] will be achieved and get high efficiency of surveillance-broadcast at sub-6 frequency, but the studied work does not describe the real characteristics of inspired metamaterial antennas rather it is conventional antennas.

An antenna inspired by metamaterial characteristics [12, 13], uses metamaterials for the size reduction of antennas and studies the properties of metamaterials. The study only considers reducing the size of an antenna and increasing gain [12]. The criteria of 5G wireless applications are addressed by the size of an antenna or by using metamaterials as an antenna, and integrating metamaterials into the mm-wave band was limited by the part of the study [13].
A metamaterial-inspired antenna intended for use in the unlicensed national information infrastructure (UNII) band in the sub-six gigahertz range has been proposed with rectangular patches transformed into u-shaped ones by cutting a slot across the middle, which increases antenna bandwidth and gain [14]. However, the study has no mathematical model for the use of different shapes of antennas. The metasurface is created to offer band-stop functionality within the antenna's operational bandwidth.

When compared to conventional antennas, the suggested technique demonstrates a mutual coupling improvement [15]. The idea to use metamaterials as a ground antenna to reduce the mutual coupling of the two antennas were analyzed. Because of air in gaps between the metasurface and antennas and the compactness of electromagnetic properties will increase the mutual coupling of an antenna. The study of [16], presents a unit cell featuring a combined EM-wave resonant mode that illustrates a near alignment of electric and magnetic responses within a particular frequency range centered around the resonance. This alignment leads to the effective wave impedance matching that of free space. Because of related resonance frequencies, interference between the two frequency bands will be high.

Small metamaterial quarter band antenna [17], as well as an ultra wide-band planar [18], are studied with an antenna's transmission lines with a right and left hand are made using unit cells of an asymmetric extended composite, which serves as the component's primary resonator and a 50Ω co-planar wave-guide as the feeding part. The designed rectangular 5G patch antenna using artificial metamaterial is designed with a two-port square microstrip antenna to resonate at 1-to-3 GHz frequency range and provided a bandwidth of 53 MHz with a reflection loss of -19.74 dB at its resonant frequency. The CST microwave studio has been used for designing the patch antenna using metamaterial structure [19]. According to the result of the study, a patch antenna will satisfy all of [17, 18, 19] results. Here, no need to use complexity to satisfy such types of antenna performance results.

In [20], the MIMO antenna for mobile terminals with extremely small effective reduced mutual couplings is to scale down the antenna size and degrade the connection between the antenna elements. Two complementary SRRs are etched on the ground plane [20]. Miniaturizing of about 60 % in the whole area of the antenna is reached, and a mutual coupling improvement of around 10 dB between those emitting radiation is observed. This paper, study about mutual coupling and reducing the size of an antenna only. To fulfill the requirements of 5G wireless applications, those components will not be satisfied and the wishes of 5G applications are not only at sub-6 frequencies.

An array of novel compact metamaterial unit cells [21], are characterized and employed for the gain enhancement of a microstrip antenna operating at 7.1 GHz. This paper [21], uses metamaterials as a superstrate of an antenna. By using this type of technique, only the gain of an antenna will be improved, but the other performance of an antenna will be as it is and an antenna operated at sub-6 frequencies.

The proposed work of the millimeter-wave metamaterials unit cell that operates at 28 GHz is presented [23]. The suggested design is a split-ring material resonator with a bandwidth of up to 1.1 GHz. However, the study covers only properties and compares the shape of metamaterials at millimeter-wave frequencies. The antenna for Ka-band [24] has very low epsilon metamaterial unit cells implanted at the plane of the antenna's aperture to increase antenna gain. Regarding frequency bands, the antenna has a complicated shape. This paper proposed only to enhance the antenna gain and has a limitation of related frequency bands, which will have mutual polarization with each other.

Asymmetric double-layer wide-band frequency Huygens' meta-surface [25], of the artificial cell, is designed for a wide-angle antenna for the next technology comings. The designed antenna has been proposed for a flat lens and does not consider the requirements for an antenna (i.e. gain, bandwidth, return loss, etc.).

Enhancing antenna power gain relies on factors such as the number of superstrates, the characteristics of the unit cell, and the separation distance between the radiation elements and the superstrates. In addition, mechanisms of designing superstrates enhance only the gain of antennas. The main drawback of using metamaterials as a superstrate is the increased size of antennas and the difficulty in manufacturing. In general, the lack of employing the meta-materials in simultaneous modes of operation, i.e., applying meta-materials as an antenna and as a ground, the antenna's performance is limited. Besides the above limitations, the existing related works also challenged

Table 2.1: Summary of Literature Review

Ref No.	**Techniques**	**Frequency bands**	**Limitations**
[10]	Metamaterials with an antenna	Sub-6 frequency	Related multiple bands, no static resonant frequency
[11]	Metamaterial loaded to antenna	Sub-6 frequency	High interference, Large VSWR
[12, 13]	Metamaterial as an antenna	Sub-6 frequency	Only for reduction of size
[17, 18, 19]	Metamaterials as part of antenna	Sub-6 frequency	Only for GSM [17], large VSWR [18], For WiMAX and GSM, but high Interference [19]
[20]	Metamaterial Loaded on antenna	Sub-6 frequency	Low efficiency
[21]	Super-strate	Sub-6 frequency	large return loss
[9]	Ground metamaterial	Sub-6 frequency	Proposed for WLAN applications only
[23]	Negative refractive	mm-wave	Unit cells properties only
[24]	Plane Metamaterial	mm-wave	Complex shape, Related frequency bands, High interference
[25]	Meta-surface	mm-wave	Meta-surface properties only
[29]	Ground metamaterial	mm-wave	Large return loss(-18dB)
[32]	Defected ground structure	mm-wave	Limited bandwidth
[33, 36, 58]	Conventional material	mm-wave	High return loss [58] and low gain [33] Very limited in bandwidth [36, 58]
[39]	Metamaterial antenna	mm-wave	Limited in gain, return loss and bandwidth
[42]	MIMO antenna	mm-wave	Large in size and has cross polarization
[43]	inset feed method	mm-wave	Large in size and high return loss
[44]	EBG structure	mm-wave	High return loss
[57]	X-slot radiator	mm-wave	Limited in gain, return loss and bandwidth

mm-wave frequencies. Designing a complex shape of meta-materials made it a challenge to operate and introduce in bands of mm-wave frequencies in the previous works. The relationship between the meta-material cell and an antenna was not taken into account, even though this interaction is rather crucial for the current distribution that highly determines the operational effectiveness of the antenna.

Designing an antenna with a meta-material inspiration can be straightforward, but successful in reaching broad objectives and good performance requires further design factoring in things like feeding methods, meta-material type, the place of the slot cell, the shape of the main antenna body, etc. This work proposes meta-materials in simultaneous modes, i.e. as an antenna and as a ground technique to achieve improved performance. Further, we study the properties of meta-materials to overcome challenges with design complexity in millimeter-wave bands and operating at a higher frequency. By overcoming these challenges this thesis will overcome and help:

- Enhancing the performance of antennas by using artificial properties of meta-material.
- Making antennas compact and reduced in size without its performance degradation.

Chapter 3

3 Fundamentals of Antenna and Meta-materials

The fundamental aspects of antennas represent the foundational parameters used for the design and discussion of various antenna types, serving to define and distinguish each antenna's characteristics.

3.1 Antenna Fundamentals

As mentioned in [26], antenna fundamentals define an antenna's capabilities. As part of the antenna design process, some design parameters like return loss, the operational frequency spectrum, radiation patterns, gain, directivity, and efficiency need to be modified as required. Some of the parameters are discussed below and not all of them are necessary to describe antenna performance.

3.1.1 Antenna Gain

The measure of an antenna's radiation pattern directionality is denoted by its antenna gain. It indicates how well an antenna focuses energy in a particular direction compared to an isotropic radiator (a theoretical antenna radiating equally in all directions).

3.1.2 Directivity

Directivity quantifies the effectiveness of an antenna in concentrating or directing its emitted power in a particular direction. It measures the concentration of radiated energy in a specific angular direction, offering insights into the antenna's capability to transmit or receive signals effectively in that particular direction [26].

3.1.3 Return Loss

Return loss measures the reflected power to the source caused by impedance mismatches in the antenna system. It is usually expressed in decibels (dB) and is calculated using

the following formula:

$$\text{Return Loss (dB)} = -20 \cdot \log_{10}\left(\frac{\text{Reflected Power}}{\text{Incident Power}}\right) \tag{1}$$

A higher return loss value indicates less power is being reflected, meaning a better impedance match between the antenna and the transmission line or source. Conversely, a lower return loss suggests a higher level of reflection and potential inefficiencies in the antenna system. Return loss is an essential parameter in antenna design and optimization, as it helps ensure efficient power transfer between the source and the antenna [26]. It is particularly crucial in applications where minimizing signal loss is important, such as in wireless communication systems. Additionally, the Voltage Standing Wave Ratio (VSWR) is often used as an alternative representation of return loss:

$$\text{VSWR} = \frac{1+\rho}{1-\rho} \tag{2}$$

where:
$\rho = 10^{-\frac{\text{Return loss (DB)}}{20}}$
A lower VSWR value corresponds to a higher return loss and better impedance matching. Both return loss and VSWR are essential metrics in evaluating the performance of antennas and ensuring optimal signal transmission [26].

Typically, the Voltage Standing Wave Ratio (VSWR) serves as a measure of the degree of mismatch between an antenna and the connecting feed line. The range of values for VSWR is from one to ∞. For the majority of antenna applications, a voltage standing wave ratio of less than 2 is acceptable. The antenna has a good match, to use the technical term. Therefore, when someone states that an antenna is poorly matched, they are referring to a frequency where the VSWR value is more than two [26].

3.1.4 Bandwidth

The bandwidth of an antenna delineates the spectrum of frequencies within which the antenna can proficiently transmit or receive signals. It is like the tuning range of a radio station. A broader bandwidth means the antenna can handle a wider range of frequencies, making it versatile for different communication technologies. On the other hand, antennas with narrower bandwidths are more specialized, focusing on specific frequency ranges [26]. The bandwidth of an antenna is a key consideration in designing communication systems, ensuring compatibility with the desired frequency range and supporting efficient signal transmission or reception. In this thesis, the substrate height of 0.35 mm and a dielectric constant of 2.2 is used.

3.2 Metamaterials

3.2.1 Introduction to Metamaterials

Metamaterials are a disruptive technology that is revolutionizing the field of antennas by exceeding the limits of traditional antenna performance and design. Metamaterial-inspired antennas leverage the unique electromagnetic properties of artificially engineered materials to enhance their functionality in ways previously unattainable. Metamaterials offer antenna designers unprecedented control over the manipulation of electromagnetic waves. By carefully tailoring the structure and composition of these materials at the micro- or nanoscale, antennas can achieve properties such as negative refractive index and improved matching of impedance. These capabilities enable antennas to overcome traditional limitations and open doors to innovative solutions for various challenges in wireless communication systems.

A significant application of metamaterials in antennas is to achieve compact designs with enhanced performance. Metamaterial-inspired structures can facilitate the creation of smaller antennas while maintaining or even improving their efficiency and bandwidth. This is particularly valuable in the development of antennas for portable devices and space-constrained environments [40]. Moreover, metamaterials contribute to the creation of multifunctional antennas that can adapt to changing communica-

tion requirements. These materials enable the realization of reconfigurable antennas, allowing adjustments in frequency bands and radiation patterns to meet dynamic communication needs. The integration of metamaterials in antenna design has also paved the way for the development of unconventional antenna shapes and structures. Antennas can be engineered to exhibit properties like cloaking or reduced radar cross-section, enhancing their stealth capabilities in military applications.

3.2.2 Classifications of Metamaterials

As many researchers verify that metamaterials are categorized into two major parts by their mathematical descriptions. Double negative and single negative structures make up the first portions. The second is the band gap of the materials used to make photonic structures. Double negative and single negative materials are homogeneous, described using the idea of an effective medium, and are significantly smaller than the operating wavelength. The separation between them in the band gap of photonic structures is at least half the wavelength. Due to this matter, PBG cannot be considered homogeneous media [16], [22], and [40].

3.2.3 Epsilon-negative Metamaterials.

Epsilon-negative (ENG) metamaterials stand out as a distinctive category of engineered materials characterized by their negative electric permittivity (ϵ). In contrast to natural materials with predominantly positive electric permittivity, epsilon-negative metamaterials are meticulously designed to exhibit a negative response when confronted with a utilized electric field. This characteristic becomes particularly significant when combined with materials displaying negative magnetic permeability, resulting in the attainment of a negative refractive index. The negative refractive index gives rise to extraordinary optical phenomena, such as negative refraction, wherein light bends in the opposite direction compared to materials considered conventional. This phenomenon is mathematically expressed as:

$$n = \sqrt{\epsilon\mu} \tag{3}$$

where n is the refractive index,
ϵ is the electric permittivity and
μ is the magnetic permeability.

The engineering of epsilon-negative metamaterials allows for tailored responses to electromagnetic waves, presenting applications in subwavelength imaging. For instance, the design flexibility of epsilon-negative metamaterials is harnessed in achieving a superlens with the ability to image details smaller than the incident light's wavelength. In the domain of antenna design, the negative electric permittivity of epsilon-negative metamaterials contributes to enhancing antenna performance, miniaturization, and efficiency [9]. The effective permittivity formula is commonly used to summarize as:

$$\varepsilon_{\text{eff}} = \varepsilon \left(1 - \frac{f_p^2}{f^2}\right) \tag{4}$$

where f represents frequency, f_p is the plasma frequency, and ε is the electric permittivity. Despite their promising applications in optics, telecommunications, and antenna technology, the practical implementation of epsilon-negative metamaterials encounters challenges such as losses and fabrication complexities[3].

3.2.4 The double-negative (DNG) metamaterial

Double negative metamaterials (DNG) represent a fascinating category of engineered materials that simultaneously exhibit negative electric permittivity (ϵ) and negative magnetic permeability (μ). In the context of antennas, these unique metamaterials offer unprecedented opportunities for innovation. By harnessing both negative ϵ and μ, DNG metamaterials enable the creation of antennas with extraordinary electromagnetic properties. This includes the potential for a negative refractive index, leading to unconventional wave propagation behaviors. Antennas designed with DNG metamaterials may exhibit enhanced performance characteristics such as improved impedance matching, reduced size, and increased efficiency. Utilizing DNG metamaterials in antenna engineering represents a promising avenue for pushing the boundaries of conventional antenna design, opening new possibilities for wireless technologies. However,

challenges in material implementation, especially at higher frequencies, and potential losses in the metamaterial structure need careful consideration in practical applications. Ongoing research in this field continues to explore the full potential of double negative metamaterials in revolutionizing antenna technology [9].

3.2.5 PBG-metamaterials

Photonic Band Gap (PBG) metamaterials represent a cutting-edge class of engineered materials designed to exert precise control over the propagation of electromagnetic waves, particularly in the optical and photonic frequency ranges. These metamaterials feature periodic structures that introduce photonic band gaps, akin to electronic band gaps in semiconductors, where certain wavelengths are forbidden. Typically organized in lattice or photonic crystal patterns, PBG metamaterials offer versatile applications [46].

The utility of the creation of efficient waveguides and optical fibers facilitates the controlled manipulation of light. The design of PBG structures supports resonant cavities, enabling the development of compact and efficient optical resonators. Moreover, these metamaterials can exhibit directional band gaps, allowing selective control of light propagation. With applications ranging from enhanced light-matter interactions to optical filters and modulators, PBG metamaterials pave the way for advancements in sensors, detectors, and nonlinear optics. Their unique properties also enable the creation of super prisms, introducing significant dispersion angles. PBG metamaterials explore innovative designs and applications, particularly in quantum optics, integrated photonics, and advanced optical communications, promising effective photonic and compact devices with enhanced performance [46].

3.2.6 Metamaterial inspired antenna

The Metamaterial-Inspired Antenna presents a cutting-edge approach to antenna design, drawing inspiration from the distinct electromagnetic properties exhibited by metamaterials. These artificially designed materials, known for their capacity to control electromagnetic waves in non-traditional manners, form the basis for integrating dis-

tinct elements into antenna structures. Elements like split-ring resonators or frequency-selective surfaces, strategically integrated, confer unique attributes to the antenna. This includes achieving miniaturization through sub-wavelength resonances, improving overall performance with heightened radiation efficiency and impedance matching, broadening the operating bandwidth, and enabling precise control over the radiation pattern. The adaptability of metamaterial-inspired antennas, allowing customized designs tailored to diverse applications and operational contexts, stands out as a notable feature [48]. Beyond their intrinsic design advantages, metamaterial-inspired antennas have the potential to reshape the landscape of wireless communication and sensing technologies. By utilizing the distinctive properties of metamaterials, these antennas offer the prospect of developing more efficient and adaptable communication systems [50]. The ability to achieve miniaturization while preserving performance integrity opens up possibilities for integration into compact devices, and wearable technology. In addition, the adaptability of these antennas facilitates customization to meet the specific demands of various scenarios, promising advancements in areas such as 5G communication, radar systems, and smart sensor networks. Despite persistent challenges, the ongoing exploration of metamaterial-inspired antenna technology indicates a transformative trajectory in reshaping the capabilities and applications of contemporary wireless communication systems [51]. Metamaterial-inspired antennas often incorporate SRRs and CSRRs to achieve unconventional properties, such as enhanced performance, miniaturization, and customized electromagnetic responses. The inspiration from metamaterials allows for versatility in design, enabling adaptability to specific applications and operating environments. SRRs are ring-shaped structures with a narrow gap that exhibit resonant behavior at certain frequencies. In antenna applications, SRRs are commonly used to enhance the antenna's performance, including frequency tuning and bandwidth improvement. They are particularly useful in achieving miniaturization and controlling the resonant characteristics of the antenna [49].

Chapter 4

4 Design of Metamaterial Inspired Millimeter-Wave Antennas.

4.1 Introduction

The design of mm-wave antennas involves several criteria to ensure optimal performance. These design criteria are crucial to achieving the desired characteristics and functionality of the antenna. Here are key considerations in the design.

Resonant Frequency ($\mathbf{f}_r$): Careful consideration of the radiator's dimensions is essential to achieve resonance at the target frequency. Parameters including length, width, and substrate properties influence the resonant frequency.

Substrate Material: The selection of substrate material significantly influences antenna effectiveness. It affects the dielectric constant, substrate thickness, and loss tangent, influencing parameters such as bandwidth, efficiency, and gain.

Ground Plane Size (L & W): The ground plane beneath the radiator is crucial to the performance of the antenna. Its dimensions influence the impedance matching, radiation efficiency, and overall characteristics of the antenna.

Substrate Thickness (h): The dielectric substrate's thickness is used for supporting the radiator.

Radiator Length ($\mathbf{L}_{pl}$): The length of the radiator is usually approximately one-half the wavelength of the operating frequency. This can vary depending on the specific design and configuration of the antenna.

Radiator Width ($\mathbf{W}_{pw}$): The width is influenced by factors such as impedance matching, bandwidth, and the desired radiation pattern. For more specific dimensions, it's necessary to use design formulas based on the desired operating frequency and other performance requirements. In addition, the properties of the substrate material, such as the dielectric constant and thickness, play a role in determining the dimensions.

Feed Technique: The method used to feed the radiator, such as microstrip line feed, proximity feed, or aperture coupling, affects the impedance matching, bandwidth, and

radiation configuration.

Matching Impedance: Achieving a good match between the radiator and the feeding network is essential for efficient power transfer and maximum power radiation. This involves adjusting the dimensions and position of the feed point.

Feeding Point ($\mathbf{X}_{fp}$& $\mathbf{Y}_{fp}$): Position on the radiator where the signal is introduced. Usually specified in terms of coordinates on the radiator. Dimensions of the antenna depend on its operating frequency and design specifications. The patch antenna typically involves a metallic material mounted on a dielectric substrate.

Feeder Line Width ($\mathbf{W}_{fline}$): Width of the antenna feeder line connecting the radiator to the feed point.

Feeder Line Length ($\mathbf{L}_{fline}$): Feeder line length, is often specified to achieve the desired impedance transformation.

Inset Length ($\mathbf{I}_{l}$): Length of the inset or the gap in the radiator where the feeding line is connected.

Inset Width ($\mathbf{I}_{w}$): Inset width, specifying the distance from the edge of the radiator to the feeding point.

Feeder Width ($\mathbf{W}_{fdp}$): The radiator's width and the distance between the antenna's feed line.

Feeder Length ($\mathbf{L}_{fdp}$): The length of the gap specifies the separation between the feeding line and the radiator.

These dimensions collectively determine the characteristics of the antenna, influencing parameters such as resonant frequency, impedance matching, bandwidth, and radiation pattern. The precise values of these dimensions depend on the desired performance goals, the frequency of operation, and the specific antenna design requirements. To have a high data rate and low latency for 5G wireless applications, the selected resonant frequency for the design is 38 GHz. Unlike higher mm-wave frequencies, which can experience increased absorption due to oxygen and water vapor, 38 GHz provides a balance between atmospheric absorption and signal propagation. While higher frequencies can experience increased susceptibility to rain fade (absorption by raindrops), 38 GHz strikes a balance between rain fade and system performance. This makes it

suitable for applications where rain fades mitigation is necessary, such as terrestrial point-to-point communication links.

4.2 Design Procedure of Metamaterial Inspired Millimeter-Wave Antennas.

To design MIA, parameters such as the operating frequency of the antenna (f_r), the relative dielectric constant of the substrate (ϵ_r), and the thickness of the dielectric substrate (h) are used. The dielectric material chosen for the design is RT5880, characterized by a dielectric constant of 2.2. Also, different formulas in the paper[11], [14], [21],[32],[34] and [58] have been used respectively. The designing procedures have several steps and considerations. Here are the steps to design a proposed antennas:

1. Dimensions of the radiators and their ground plane.

The substrate thickness was established using the following relationship.

$$h \leq \frac{0.3c}{2\pi f\sqrt{\varepsilon_r}} \leq \frac{0.3 \times 3 \times 10^8}{2\pi \times 38 \times 10^9\sqrt{2.2}} \leq \underline{2.541 \text{ mm}} \tag{5}$$

Taking into account the result provided in equation 5, the RT Duroid 5880 laminate was selected as a substrate, with a thickness of $h = 0.35$ mm, permittivity $\varepsilon_r = 2.2$, and $\tan\delta = 9.0 \times 10^{-4}$. In the next calculation step, the width of the radiating element should be determined from the following relationship.

$$W_{pw} = \frac{c}{2f_r}\sqrt{\frac{2}{\varepsilon_r + 1}} = \frac{3 \times 10^8}{2 \times 38 \times 10^9}\sqrt{\frac{2}{2.2 + 1}} = \underline{3.12 \text{ mm}} \tag{6}$$

It is necessary to compute the substrate's effective permittivity $\varepsilon_{\text{reff}}$ before determining the radiating element's length. It is defined by the following relationship.

$$\varepsilon_{reff} = \frac{\varepsilon_r + 1}{2} + \frac{\varepsilon_r - 1}{2\sqrt{1 + 12\frac{h}{W_{pw}}}} = \frac{2.2 + 1}{2} + \frac{2.2 - 1}{2\sqrt{1 + 12 \times \frac{0.35}{3.12}}} = 1.6 + 0.3917 = \underline{1.9917} \tag{7}$$

Upon calculating $\varepsilon_{\text{reff}}$, the effective length of the patch Le should be determined from the following relationship.

$$L_e = \frac{c}{2f_r\sqrt{\varepsilon_{\text{reff}}}} = \frac{3\times10^8}{2\times38\times10^9\sqrt{1.9917}} = \underline{2.797\text{ mm}}. \tag{8}$$

Then, to calculate how much the radiator should be reduced the following relationship will be used.

$$\Delta L = \frac{0.412\cdot h\left(\varepsilon_{\text{reff}}+0.3\right)\left(\frac{W_{pw}}{h}+0.264\right)}{\left(\varepsilon_{\text{reff}}-0.258\right)\left(\frac{W_{pw}}{h}+0.8\right)} \tag{9}$$

$$= \frac{0.412\times0.35(1.9917+0.3)\left(\frac{3.12}{0.35}+0.264\right)}{(1.9917-0.258)\left(\frac{3.12}{0.35}+0.8\right)} = \underline{0.18\text{ mm}}. \tag{10}$$

The final patch length value is:

$$L_{pl} = L_e - 2\Delta L = 2.797 - 2\times0.18 = \underline{2.437\text{ mm}}. \tag{11}$$

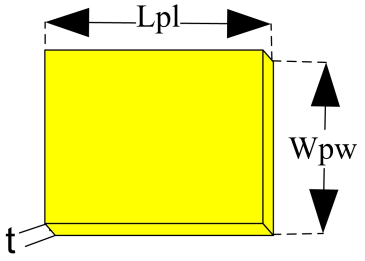

Figure 4.1: The dimension of radiator antenna part

The patch thickness, t is chosen to be very thin such that t $<<$ λ_0, and for this case, it is selected at t = 0.035 mm which is one of the standard thickness dimensions at mm-Wave frequency.

$$L = L_{pl} + 6h = 2.437 + 6\times0.35 = \underline{4.537\text{ mm}}. \tag{12}$$

$$W = W_{pw} + 6h = 3.12 + 6\times0.35 = \underline{5.22\text{ mm}}. \tag{13}$$

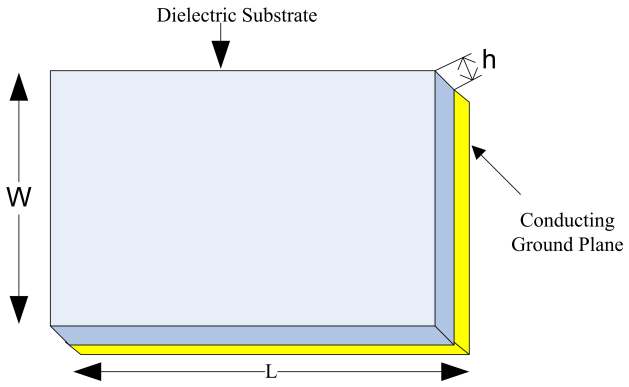

Figure 4.2: The ground plane

2. The feeding point of antennas on the X−Y coordinates. The feeding point can be located at the point (X_{fp}, Y_{fp}) in the x-y coordinates and will be calculated as follows:

$$X_{fp} = \frac{Lpl}{2\sqrt{\varepsilon_{\text{reff}}}} = \frac{2.437 \text{ mm}}{2\sqrt{1.9917}} = \underline{0.8634 \text{ mm}}. \tag{14}$$

$$Y_{fp} = \frac{W_{pw}}{2} = \frac{3.12 \text{ mm}}{2} = \underline{1.56 \text{ mm}}. \tag{15}$$

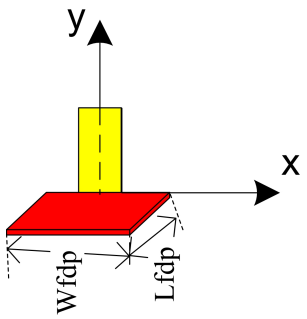

Figure 4.3: The proposed antenna feeder point and dimension

3. Matching impedance.

The maximum power transfer is achieved at the matched impedance of the load and the source of an antenna.

$$\mathrm{Z_p} = 90\left(\frac{\varepsilon_\mathrm{r}^2}{\varepsilon_\mathrm{r}-1}\right)\left(\frac{\mathrm{L_{pl}}}{\mathrm{W_{pw}}}\right)^2 = 90(\frac{2.2^2}{2.2-1})(\frac{2.437}{3.12})^2 = \underline{221.43\Omega}. \tag{16}$$

The quarter wave impedance of the radiators has been calculated from patch impedance

by:

$$\mathrm{Z_{qtr}} = \sqrt{\mathrm{Z_0 * Z_p}} = \mathrm{Z_{qtr}} = \sqrt{50\Omega * 221.43\Omega} = \underline{105.22\Omega}. \tag{17}$$

To calculate the width of the patch antenna feeder line, the impedance of the feeder line is first calculated.

$$\mathrm{Z_{(fline)}} = \frac{120\pi\sqrt{\varepsilon_{\mathrm{reff}}}}{\frac{\mathrm{W_{pw}}}{\mathrm{h}} + 1.393 + 0.667\,\mathrm{In}\left(\frac{\mathrm{W_{pw}}}{\mathrm{h}} + 1.44\right)}, \frac{\mathrm{W_p}}{\mathrm{h}} > 1 \tag{18}$$

$$\mathrm{Z_{(fline)}} = \frac{120\pi\sqrt{1.9917}}{\frac{3.12}{0.35} + 1.393 + 0.667\ln\left(\frac{3.12}{0.35} + 1.44\right)} = \underline{44.836\Omega}. \tag{19}$$

Where W_{pw} is the width of the designed antenna, h is the substrate's thickness, and $\varepsilon_{\mathrm{reff}}$ is the effective dielectric constant.

4. Dimensions of the feeder line for radiation.

The next step is to calculate the width of the microstrip patch feeder line as follows: By assuming the calculated impedance as the characteristic impedance of the feeder line (i.e. $Z_{fline} = Z_0$), the width of the feeder line will be.

$$W_{fline} = \frac{5.98h\left(\frac{1}{e^{\left(\frac{Z_0\sqrt{\varepsilon_{\mathrm{reff}}}+1.41}{87}\right)}} - t\right)}{0.8} \tag{20}$$

$$W_{fline} = \frac{5.98 * 0.35mm\left(\frac{1}{e^{\left(\frac{44.836\sqrt{1.9917}+1.41}{87}\right)}} - 0.035mm\right)}{0.8} = \underline{0.92mm}. \tag{21}$$

The length and the width of the proposed patch antenna feeder line will be calculated as:

$$\mathrm{L_{fline}} = \frac{\lambda_0}{4 * \sqrt{\varepsilon_r}} = \frac{7.895\ \mathrm{mm}}{4 * \sqrt{2.2}} = \underline{1.33\ \mathrm{mm}}. \tag{22}$$

5.Inset dimension.

The slotted gap in the patch antenna determines its resonance frequency. The following equation represents the relationship between the inset gap and resonance frequency of 38GHz:

$$\mathrm{I_w} = \frac{4.65 * 10^{-3} * \mathrm{C_0}}{\mathrm{f_0}\sqrt{2 * \varepsilon_{\mathrm{reff}}}} = \frac{4.65 * 10^{-3} * 3 \times 10^8}{38 \times 10^9\sqrt{2 * \varepsilon_{\mathrm{reff}}}} = \underline{0.0184mm}. \tag{23}$$

Here, C_0 is the speed of light and $\varepsilon_{\text{reff}}$ is the effective dielectric constant.

$$\mathrm{I_l} = \frac{L_{pl}}{\pi} cos^{-1} \sqrt{\frac{Z_0}{Z_l}} = \frac{2.437}{\pi} cos^{-1} \sqrt{\frac{50}{105.22}} = \underline{0.6285mm}. \tag{24}$$

6. Feeder dimension.

The width of the feed point is calculated using the equation given by:

$$W_{fdp} = \frac{2\mathrm{h}}{\pi} \left[([\mathrm{B}-1] - \ln[2\ \mathrm{B}-1]) + \left(\frac{\varepsilon_{\mathbf{r}}-1}{\varepsilon_{\mathbf{r}}} \left[\ln[\mathrm{B}-1] + 0.39 - \frac{0.6}{\varepsilon_{\mathbf{r}}} \right] \right) \right] \tag{25}$$

Where, h is substrate height, ε_r is dielectric constant, and B is constant. However, B and Z_{fdr} are calculated before calculating the width of the feed point. Therefore, Z_{fdr} is calculated by using equation below and B is calculated by:

$$\mathrm{B} = \frac{60\pi^2}{\mathrm{Z}_{fline}} \sqrt{\varepsilon_{\mathbf{r}}} = \frac{60\pi^2}{44.836\sqrt{2.2}} = \underline{8.905}. \tag{26}$$

By substituting the value of B.

$$W_{fdp} = \frac{20.35\mathrm{mm}}{\pi} \left[([8.905-1] - \ln[2(8.905)-1]) + \left(\frac{2.2-1}{2.2} \left[\ln[8.905-1] + 0.39 - \frac{0.6}{2.2} \right] \right) \right] \tag{27}$$

$$W_{fdp} = \underline{1.1323mm}. \tag{28}$$

Also, the length of the feed point is calculated as follows:

$$\lambda_{eff} = \frac{\lambda_0}{\sqrt{\varepsilon_{\mathbf{r}}}} = \frac{7.895}{\sqrt{1.9917}} = \underline{5.594mm}. \tag{29}$$

$$L_{fdp} = \frac{\lambda_{eff}}{4} = \frac{5.594}{4} = \underline{1.3985mm}. \tag{30}$$

Figure 4.4 shows the designed proposed work based on the equation parameters calculated from equation 5-30.

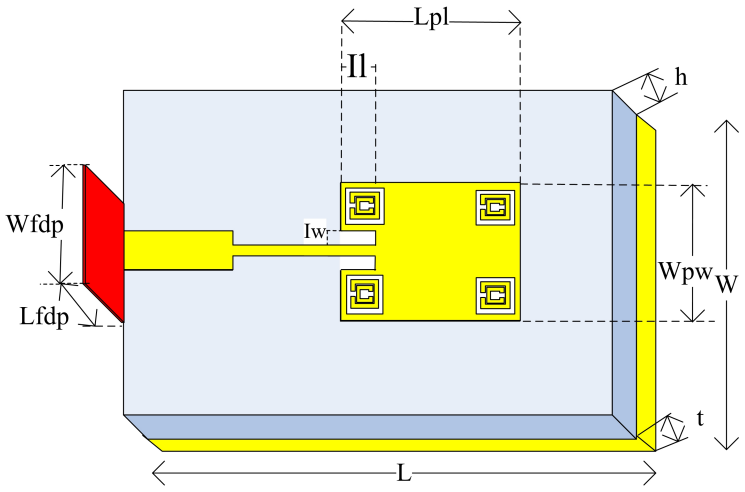

Figure 4.4: The proposed MIA specifications.

4.3 Design of Single Metamaterial Inspired Millimeter-Wave Antennas.

This designed work is simulated and analyzed by CST Studio Suit. The procedure for designing a single unit-cell metamaterial antenna is the following:

- Determine operational frequency;
- Determine the ring thickness;
- Determine the ring's separation space.

To improve antenna performance, the new structure that integrates the SRR slots into the radiator and the ground plane were presented. In this approach, since the properties of electric and magnetic fields are used to select meta-materials, changing these fields can cause the MPA's characteristics to change so that performance can be improved without increasing the physical size or the losses. Inspired by this new idea, a unit cell of basic meta-materials developed by SRR is shown in Figure 4.6. As illustrated in this figure, there is an air gap between the outer and inner rings of the SRR, resulting in different resonant frequencies. To determine these frequencies and the physical dimensions of the proposed SRR structures, the following procedure will be employed. Suppose that L denotes the length and L_o, L_i are the outer and inner lengths, respectively. Then the lengths L_1, L_2 can be calculated using equations 31a

and 31b [2] [3], respectively.

$$L_1 = 4(L_o - R_{\text{thck}}) - R_{\text{gp}}, \tag{31a}$$

$$L_2 = 4(L_i - R_{\text{thck}}) - R_{\text{gp}}, \tag{31b}$$

where $R_{\text{thck}}, R_{\text{gp}}$ denote the thickness of the rectangle and the gap, respectively. To calculate Lo and Li, we first find the outer width and length of the substrates. Hence, the two resonant frequencies of the proposed SRR will be 30 GHz and 46 GHz to get the averages of 38 GHz. Further, the length L_1, L_2 can be computed as:-

$$L_1 = \frac{c}{2f_{outer}\sqrt{\epsilon_{\text{r}}}} = \frac{3 \times 10^8 m/s}{2 \times 30 \times 10^9 hZ\sqrt{2.2}} = \underline{3.4mm}, \tag{32a}$$

$$L_2 = \frac{c}{2f_{inner}\sqrt{\epsilon_{\text{r}}}} = \frac{3x10^8 m/s}{2 \times 46 \times 10^9 hZ\sqrt{2.2}} = \underline{2.1mm}, \tag{32b}$$

respectively, where c denotes the speed of light ($\approx 3.0 \times 10^8 m/s$). After the L1 and L2 parameters, the outer and inner lengths of the SRR radiators have been calculated. To obtain uniform slotted gaps we have selected R_{thck} and R_{gp} is equal to the inset length of the radiators (e.i, I_l=0.15mm) as the optimized design in Figure 4.5.

$$L_o = \frac{(L_1 + 4R_{\text{thck}}) + R_{\text{gp}}}{4} = \frac{(3.4 + 4 * 0.15) + 0.15}{4} = \underline{1.0375mm}, \tag{33a}$$

$$L_i = 4(L_i - R_{\text{thck}}) - R_{\text{gp}} = \frac{(2.1 + 4 * 0.15) + 0.15}{4} = \underline{0.7mm}, \tag{33b}$$

The gap G_p between the two inner rings is calculated as follows:

$$G_p = \frac{L_o - (l_i + 2R_{thck})}{2} = \frac{(1.0375 - 0.7 - 2 * 0.15)}{2} = \underline{0.0187mm} \tag{34a}$$

The ϵ_{eff} is computed as

$$\epsilon_{\text{eff}} = \frac{\varepsilon_r + 1}{2} + \frac{\varepsilon_r - 1}{2\sqrt{1 + 12\frac{h}{L0}}} = \frac{2.2 + 1}{2} + \frac{2.2 - 1}{2\sqrt{1 + 12\frac{0.35}{2.1}}} = \underline{1.95mm}, \tag{35}$$

where ε_r is permittivity and h denotes the substrate thickness. When two resonators with two different resonant frequencies at L_i and L_o are coupled, the coupling changes

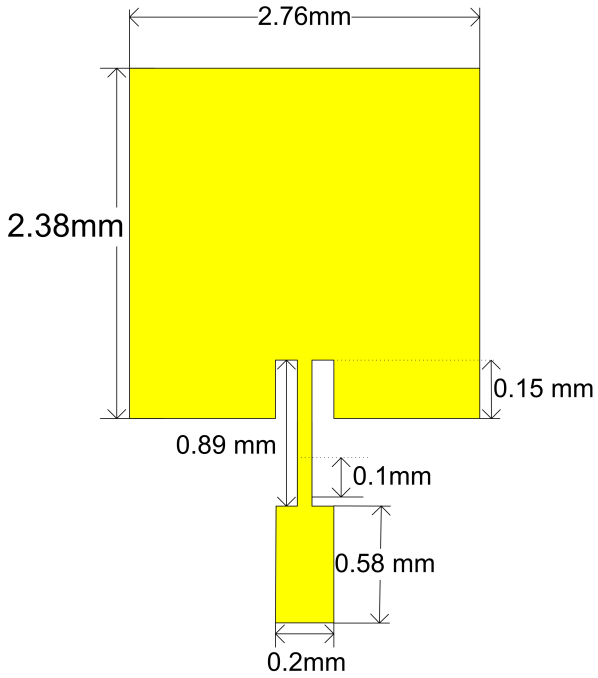

Figure 4.5: Rectangular microstrip antenna.

both resonances by f_o. The frequency variation depends on the coupling values between the two rings and the resonant frequency of each loop occurs at half-wavelength, which can be determined as

$$f_{\mathrm{o}} = \frac{c}{2L_{\mathrm{eq}}\sqrt{\epsilon_r}} \approx \underline{38GHz}, \tag{36}$$

where $L_{\mathrm{eq}} = \frac{L_1+L_2}{2}$.

As such, the SRR slot designed with the above equation was implemented on both the ground and the radiator parts of the antennas. This leads to low loss properties by reducing the reflection coefficient, impedance matching, and other losses, such as surface wave and spurious wave losses. A single conventional antenna and metamaterial unit cells were then added, to achieve more performance without degrading the previous antenna performances. The added metamaterial unit cells have the property of SRR, which has a negative refractive index, negative permeability, and permittivity to get a backward wave that produces better radiation from the antenna's high performance. Figure 4.5 shows the front view of the proposed rectangular MPA. Table 4.1 displays the suggested antenna measurements. As shown in the table the size of MPA

Table 4.1: Specifications of the computed antenna configuration.

Antenna Component	Symbol	Calculated Dimensions (mm)	Optimized dimensions (mm)	MIA dimensions
Ground-plane width	W	5.22	5.22	5.22
Ground-plane length	L	4.537	4.537	4.537
Patch width	W_{pw}	3.12	2.76	2.6427
Patch length	L_{pl}	2.437	2.38	2.2827
Copper thickness	C_u	0.035	0.035	0.035
Substrate-thickness	h	0.35	0.35	0.35
Permittivity	ϵ_r	2.2	2.2	2.2
Effective Permittivity	ϵ_{eff}	1.9917	1.9917	1.9917
Inset feed gap	I_l	0.6285	0.15	0.2
Inset feed length	I_w	0.0184	0.05	0.05
Width of feed point	L_{fdp}	1.1323	1.52	1.52
Length of feed point	W_{fdp}	1.3985	0.95	0.95
Width of feeder line	W_{fline}	1.33	0.95	0.95
Length of feeder line	L_{fline}	0.92	0.2	0.2

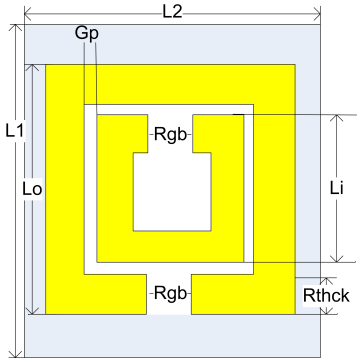

Figure 4.6: The unit cell of SRR metamaterials

and MIA were 2.76mmx2.38mm and 2.6427mmx2.2827mm respectively. This means that the size of MIA is reduced by 8% when compared with conventional antennas.

To improve the efficiency of antennas, the introduction of SRR metamaterials which has a properties of negative refractive indexes are suggested. The propagation capabilities of electric and magnetic waves through MIAs radiators has been enhanced via a proposed SRRs. Therefore, to achieve the requirements of 5G wireless applications like data rates, flexibility, and bandwidhths, SRR metamaterials which are shown in Figure 4.6 were proposed.

The SRR as shown in Figure 4.6 is the proposed metamaterial to be introduced in

Table 4.2: Calculated Dimensions of the unit cell SRR metamaterial design.

SRR Component	Symbol	Calculated (mm)	Optimized(mm)
Outer Length	L_o	1.0375	0.5
Inner length	L_i	0.7	0.45
Gap	R_{gp}	0.15	0.05
Thickness of rectangle	R_{thck}	0.15	0.05
gap between rectangle	G_p	0.0187	0.025

the ground of the antenna and on the radiator part. To obtain a low-loss antenna by reducing the reflection coefficient, impedance matching, and different losses such as surface wave loss and spurious wave losses, the placement and design of SRR have been proposed. The reason for the low bandwidth of antennas are in part due to the surface wave loss and the different drawbacks of antennas. In MPA to obtain wider bandwidth, the thickness of the antenna substrate must increase. However, the thickness of the substrate will generate surface loss and spurious loss in MPAs; this will degrade the performance of MPA that are needed in 5G wireless applications. Therefore, to decrease these types of losses and enhance antenna performance, the design and structure modification as the proposed work is the solution.

4.4 Mutual coupling of MIA

To reduce mutual coupling and interconnected radiation of different antennas; metamaterial SRRs have been used and designed. The effects of mutual coupling between antenna elements include matching properties, antenna efficiency, correlation, and radiation pattern. The designed SRR unit cell metamaterial is placed in reasonable ways to reduce the drawbacks of rectangular MPAs as shown in Figure 4.8. Figures 4.8(a)-(d) depict the design steps for a single-element MIA. In this structure, the metamaterial SRR slot placement is technically selected to regulate the current distribution of antennas. As can be seen from the figure, the SRR slot is introduced on the upper and lower parts of the radiator; in such a way it enhances the antenna performance. More specifically, the metamaterial SRR slot introduced in Figure 4.8(b) is used to alter and then enhance the magnitude of the fringing fields from the radiator to the

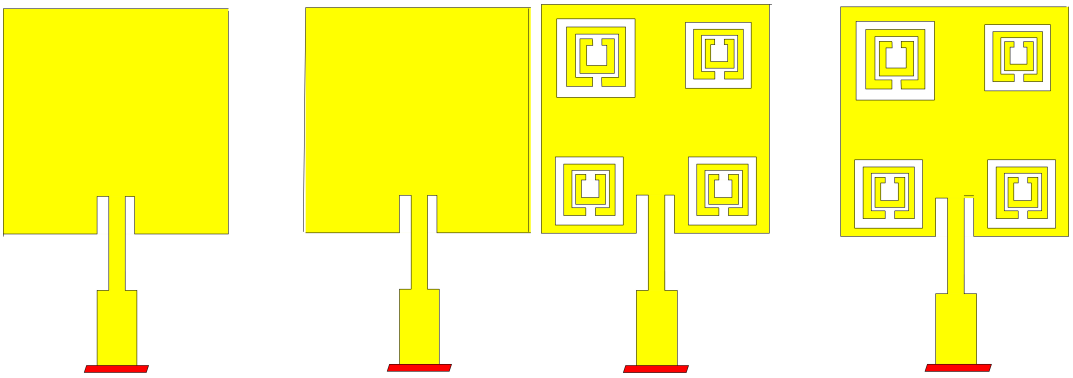

(a) Mutual coupling of MPA (b) Mutual coupling of MIA

Figure 4.7: The mutual coupling of different antenna types.

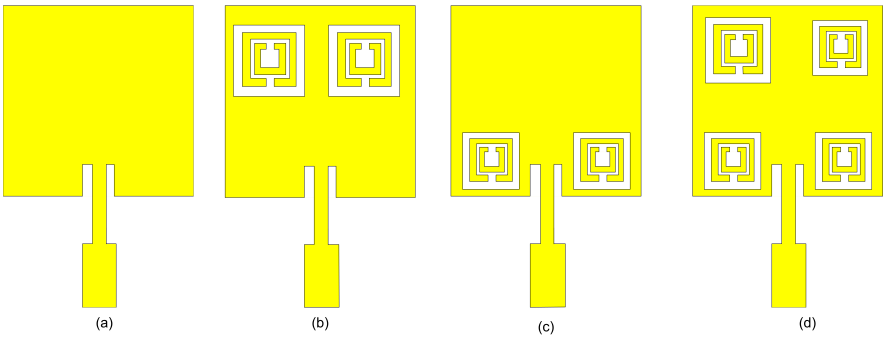

Figure 4.8: The design steps of radiator parts.

space. Next, the structure in Figure4.8(c) is developed to minimize the returned power to the source and regulate the flow and path current distribution at the feeding edge of MPAs. Finally, an MIA that can achieve improved performance is constructed by integrating the structures from previous steps, as shown in Figure 4.8(d). To reduce the main drawbacks of rectangular MPAs like surface wave loss and spurious wave loss, SRR metamaterials were added at the ground of the radiator as shown in Figure 4.9 and the more performed of Figure 4.10 has been selected.

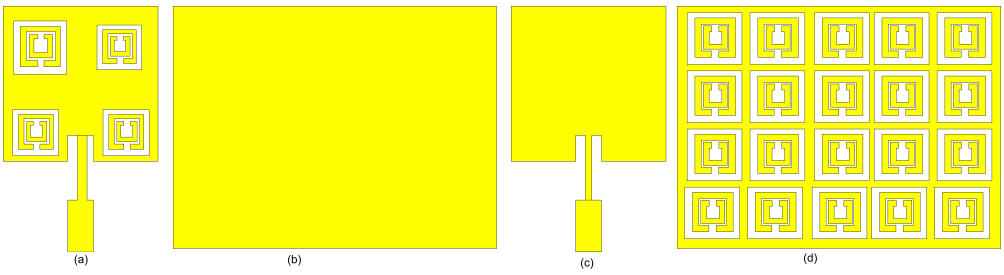

Figure 4.9: Design steps of ground MIA with radiator parts.

4.5 Design of Linear Metamaterial Inspired Millimeter-Wave Antennas.

Figure 4.10 of the rectangular MPA was inspired by 2x2 in the front view and 4x5 SRR array meta-materials in the ground of the antenna.

In Figure 4.11 the 2x1 of MIA array has a size of 8mmx4.54mm with 4x6 SRR structure

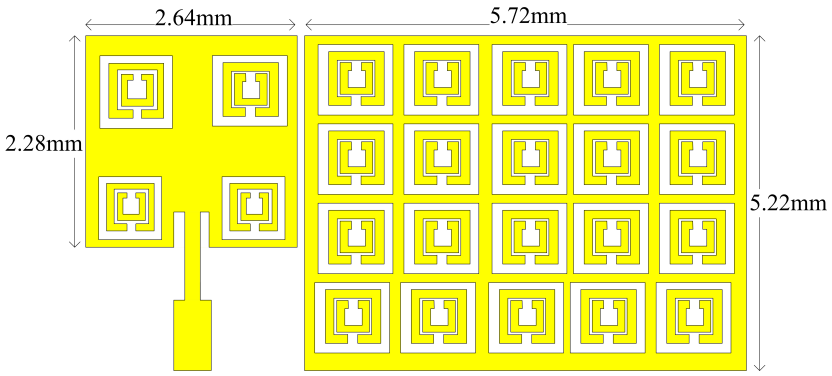

Figure 4.10: The selected design element of the meta-material inspired antenna (MIA).

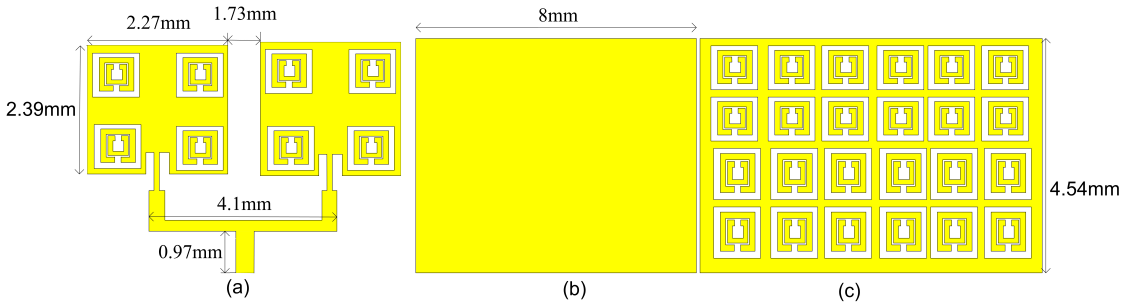

Figure 4.11: 2x1 of MIA (a, without(b), and with added ground of 4x6 SRRs (c).

slots at the ground. The connector between the two radiator elements has a length of 4.1mm and 50Ω impedance and the distance between the two internal antennae has a space length of $\lambda/4$ which is optimized to 1.73mm by CST Microwave Simulators. In a conventional MPA, the minimum internal element space is $\lambda/2$. This is to decrease the level of the minor lobe of an antenna. However, the width of the main lobe antenna collapsed as the space antenna element increased.

Figure 4.12 shows the 4x1 MIA arrays with a radiator and ground size of 2.47mm x 2.35mm, and 17mm x 7.5mm respectively. The SRR metamaterial slot has been added to inspire and motivate the efficiencies of the radiators by 16x7 SRR matrices. The

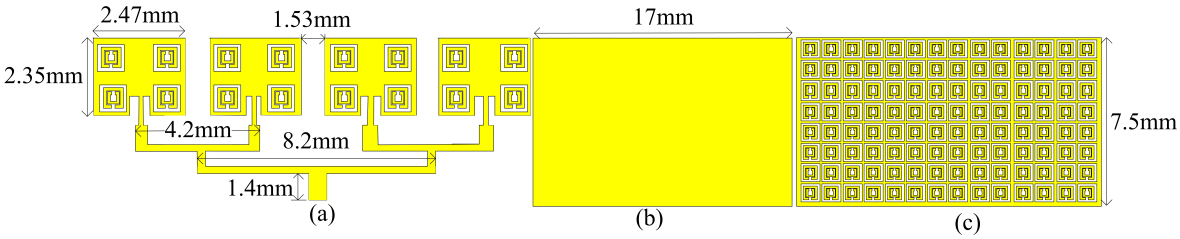

Figure 4.12: 4 x 1 metamaterial inspired millimeter-wave antenna arrays (a), Without (b) and with 16 x 7 SRRs (c).

rest of the designed 2x1, and 4x1 MIA indicated parameters are according to appendix Table 7.2 and 7.3. The side lobe level and main lobe magnitudes are considered when SRRs are inspired by the proposed works. In this paper, metamaterial SRR structure slots are used rather than increasing the internal space of each antenna to decrease the side lobe level in addition to getting the wider main lobes. This also improves the compactness of 5G wireless communication antennas by not only decreasing the size of radiators but also reducing the whole antenna dimensions.

4.6 Design of Planar Metamaterial Inspired Millimeter-Wave Antennas.

Planar design of antennas is the latest antenna design, which has attractive qualities such as low profile, lightweight, affordable price, and simplicity of array integration. These components are ideal for modern communication systems, particularly for applications in cellular 5G networks, owing to their distinctive characteristics. An antenna with a planar array of its elements is both active and parasitic in one plane. A planar array antenna has a large aperture and can be used to adjust the relative phase of each member to change the direction of the beam and is frequently utilized in 5G communications and radar systems. Planar arrays of printed radiating elements make excellent choices for applications requiring low-cost scanning arrays. Because they can be utilized to create patterns that cannot be produced by a single element and linear arrays of antennas. They are also utilized to improve directivity and perform numerous additional tasks that would be challenging with linear arrays. Linear metamaterial millimeter-wave antennas with the above-mentioned architecture have only been utilized to scan in one direction. However, in many situations, it will be necessary to

use antenna arrays that can scan in both dimension planes, which means, in the elevation and azimuth plane. To fulfill those requirements, planar metamaterial-inspired millimeter-wave antennas have been designed and proposed as shown below. In Figure

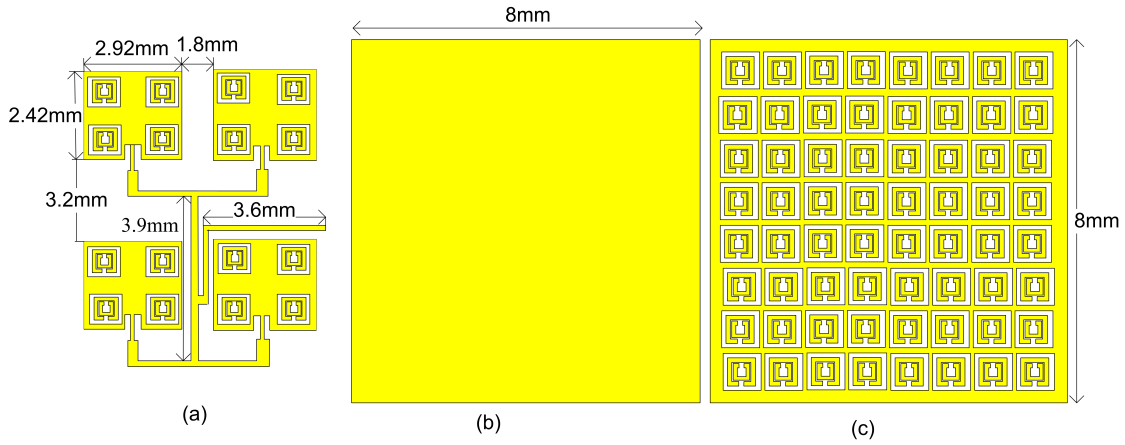

Figure 4.13: 2x2 of MIA (a), without (b), and with the added ground of 8x8 SRRs (c).

4.13 the designed 2x2 of MIA with 16 on the radiator and 8x8 structure slots on the ground of the antenna respectively. The 3.6mm length with an impedance of 100Ω feeds the 2x2 MIA. The 2x1 connector length is 3.9mm with an impedance of 50Ω, which is used to regulate and match the current flow between the two branches. The size designed 2x2 MIA has a compact size (8mm x 4.54mm) with any device with a very good profile, saving materials, and easily designed scenarios. The Figure shown in 4.14

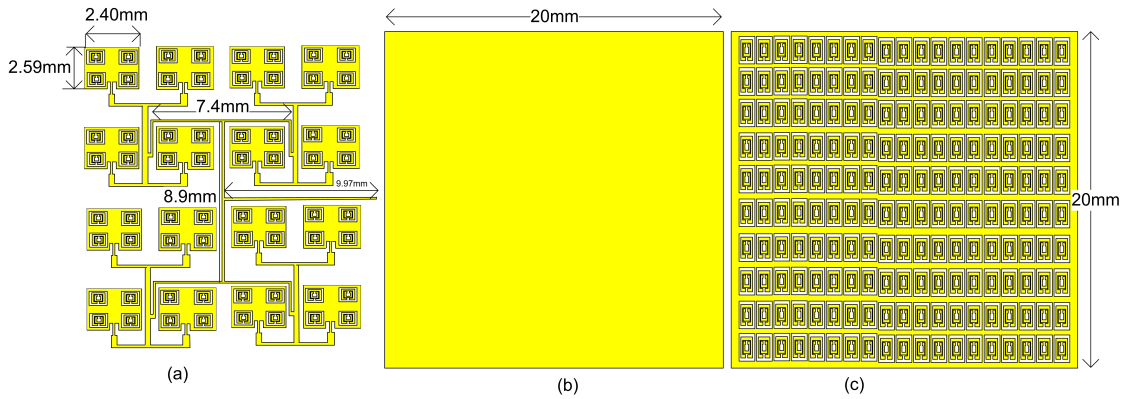

Figure 4.14: 4x4 of MIA (a), without (b), and with the added ground of 19x19 SRRs (c).

is the designed 4x4 MIA arrays with a size of 2.4mm x 2.59mm for the radiators and 20mm x 20mm for the radiators ground respectively. Here, the 2x2 MIA arrays are the main starting to design. The power divider of the 2x2 MIA arrays is 7.4mm and the

4x2 MIA connectors have a length of 8.9mm with 100Ω impedance matching. Figure

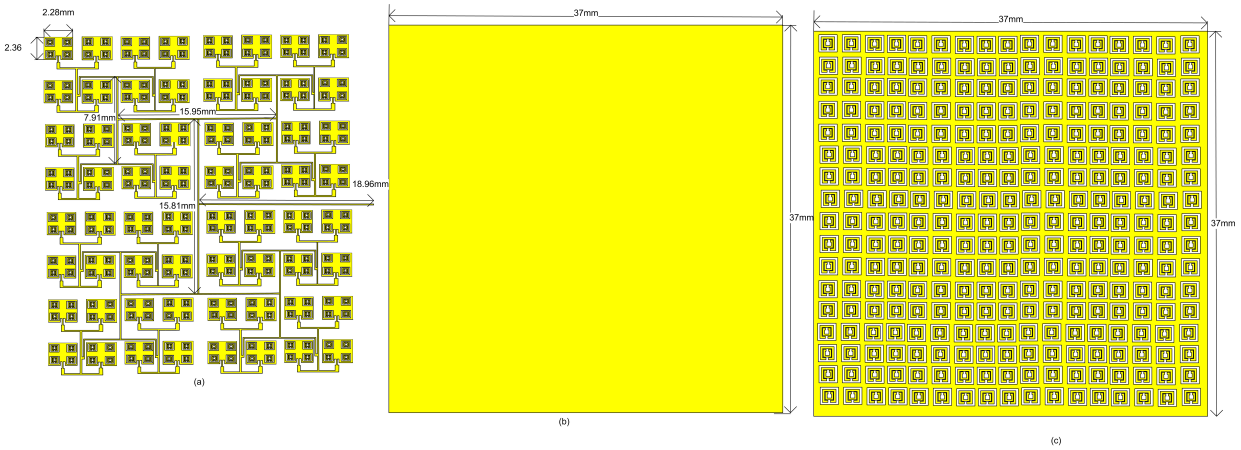

Figure 4.15: 8x8 of MIA (a), without (b), and with the added ground of 17x17 SRRs (c).

shown in 4.15 were the 8x8 MIA arrays which were designed on the substrate area of 37mm x 37mm with a single radiator size of 2.28mm x 2.36mm. The number of SRRs is 17x17 on the ground plane of the radiators. Also, the rest of the specific parameters are based on the appendix of Table 7.6. The SRR metamaterial unit cell was placed at a distance of 1mm from each other, to reduce the mutual coupling between antenna elements. Higher bandwidth, gain, directivity, and radiation efficiency were achieved by using metamaterial at the ground of antenna arrays. When the metamaterial is loaded with the ground, it will act as a reflecting surface and it will focus the maximum radiation energy in the desired direction. Also, it inhibits the surface wave of an antenna, leading to significant enhancements in both return loss and VSWR. However, the loss caused by surface waves in the antenna mostly affects antenna arrays [23].

4.7 Fringing of electric fields along the proposed patch antenna

In this subsection, the reason why the proposed MIA design can achieve improved performance at high frequencies such as 38 GHz were presented. The performance of MIA is significantly affected by the magnitude of the fringing fields. Figure 4.16 demonstrates the impacts of a metamaterial unit cell (SRR) on the fringing area of an MIA. Since there is no fringing of electric fields along the length of the patch, the radiation caused by the fringing field that occurred between the MIA's edge and the

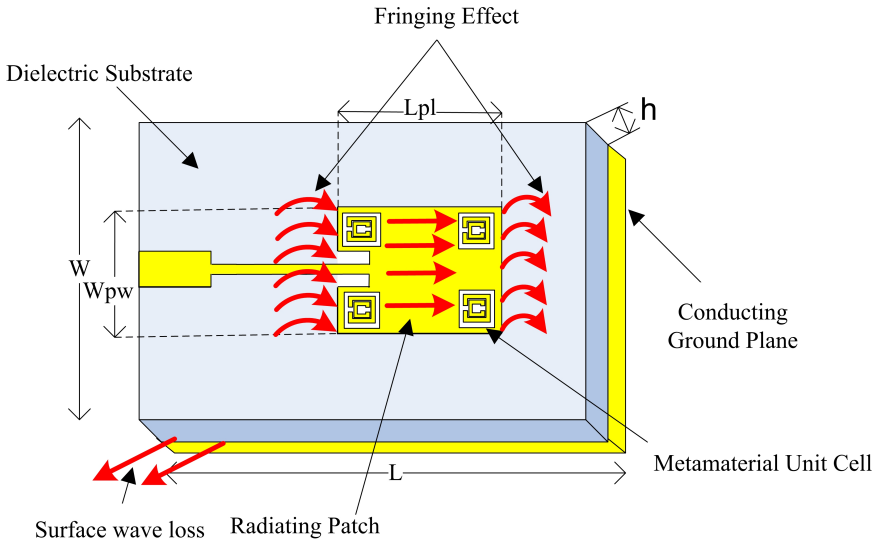

Figure 4.16: Effect of Meta-material unit cell on the fringing area of MIA.

ground plane (along the width of the patch) would be used for communication purposes. Furthermore, the magnitude of the fringing field is affected by the MIA size and substrate height. Technically, the fringing field gets higher as the height of the substrate increases. An MIA would appear electrically broader in comparison to its physical part due to the fringing effect. Thus, it is necessary to increase the fringing effect of MIAs to attain antennas with good performance for efficient radio propagation, and the meta-materials have a great role in increasing the fringing effects. As shown in Figure 4.10, the unit cell meta-material was applied to the patch. Altering the current distribution pattern and lowering the high input impedance of the standard patch antenna, significantly raises the amount of current that reaches the radiating patch's center and edge. This lengthens the effective length of the radiator and helps it radiate the input power strongly. From an alternative angle, it is intended for the SRR meta-materials loaded at the antennas' ground to function as a reflecting surface, concentrating the most radiation energy in the intended direction. Additionally, it reduces the antenna's surface wave loss, which greatly improves the returned loss and VSWR. Therefore, antenna performance parameters like radiation efficiency, gain, bandwidth, and directivity are increased by using the suggested strategy at the effective fringe area.

Chapter 5

5 Simulation results and discussions

In this chapter, the performance analysis of MIA has been simulated using CST-MW and then analyzed. The simulation result was done to analyze and enhance antenna performance like VSWR, return loss, Bandwidth, directivity, gain, and radiation efficiency. First, the SRR metamaterial unit cell has been analyzed and simulated for the sake of determining the SRR properties and enhancing the performance of different antenna types by introducing the SRR to its radiators and ground plane respectively. Then after, the 2x1, 4x1, 2x2, 4x4, and 8x8 MIA arrays have been simulated and analyzed.

5.1 Simulation results of SRR metamaterial

Figure 5.1 (a) shows the real and imaginary parts of the reflection (S11) and transmission (S21) coefficient of the SRR slot. Permittivity and permeability properties of the SRR slot are extracted from S-parameters. From the simulated result depicted in Figure 5.1 (b), the plot's magnitude is clearly within the negative and positive regions for permittivity and permeability, respectively. In conventional scenarios, this plot characteristic is not obtained or exists. Thus, the designed SRR slot exhibits permittivity and permeability characteristics, which is important to enhance the antenna performances.

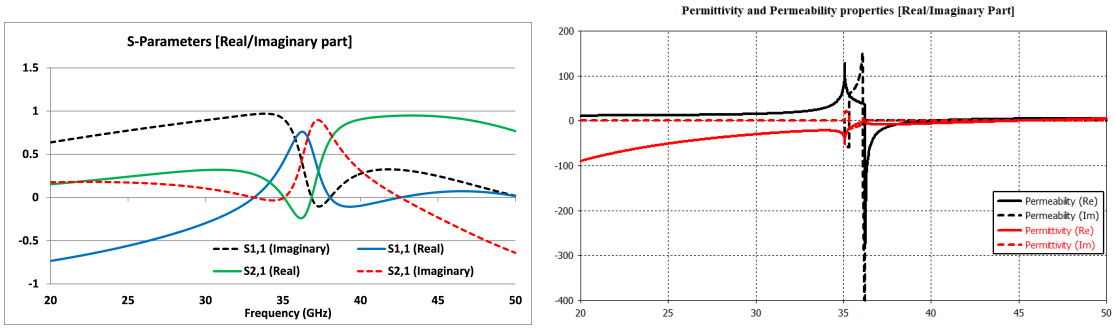

(a) S-parameters (Real and imaginary parts) of Meta-material SRR slot.

(b) Permittivity and Permeability of Meta-material SRR slot.

Figure 5.1: The simulated parameters of SRR slots.

A negative refractive index makes a backward wave which produces better radiation from the antenna resulting in low loss [30].

5.2 The mutual coupling results of MPA and the proposed MIA antennas

Figure 5.2 is the mutual coupling simulation results of an MPA and MIAs shown in Figure 4.7, which was designed with the same orientation and distance between two antenna elements. Based on the results of both Figure 5.2 (a) and (b) the proposed work has a very limited mutual coupling in regards to conventional antennas. The gain, propagation, and antenna pattern can all be negatively impacted by the mutual coupling of energy that results from the proximity between two elements. This issue can cause the designed antenna to deviate from reality and occasionally even become unbearable. By the results of Figure 5.2 (a) and (b), the MIA has better performance than the traditional antennas with a mutual coupling difference of 8.81dB (i.e, -19.9 dB of MPA, and -28.71 dB of MIA).

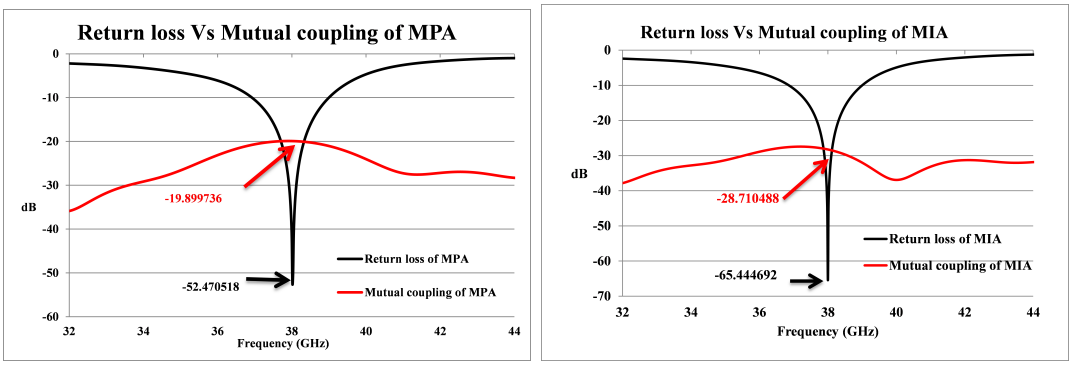

(a) The return loss vs mutual coupling of MPA

(b) The return loss vs mutual coupling of MIA

Figure 5.2: The return loss vs mutual coupling of different antenna designs.

5.3 The Simulation results of the proposed MIA antennas

Figure 5.3 shows the return loss of -57.42 dB for MPA and a bandwidth of 2.081 GHz. This result has a higher performance than conventional antennas. But, if SRR meta-

material unit cells have been applied it will highly achieve the requirements of 5G wireless applications. The return loss result of the rectangular microstrip antenna was enhanced by using an SRR meta-material unit cell as the antenna part and ground from -57.42dB to -82.95dB and has a bandwidth of 1.971GHz which is an MIA. The enhanced return loss has a change of -25.53dB. This shows that meta-material unit cells are inserted in the proper place and have a great role in enhancing the performance of antennas.

In Figure 4.8, steps (b) and (c) have been designed to show the meta-material place-

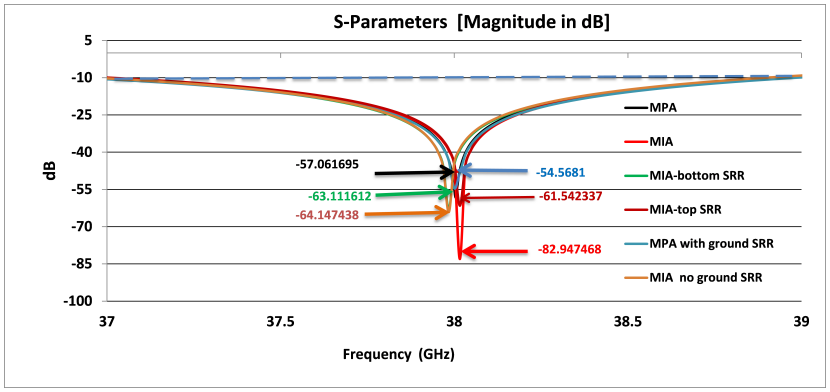

Figure 5.3: The return loss of different antenna designs.

ment effect on antenna performance and see the result in Figure 5.3 (i.e. MIA top SRR and MIA bottom SRR). As the result shows that the bottom and top SRR meta-material-inspired antenna has a large return loss compared with 2x2 SRR-inspired meta-materials. The primary purpose of the upper SRR is to augment the fringing fields emitted by the patch. The significance of these fringing fields lies in their essential contribution to the radiation mechanism. The bottom SRR induces a magnetic field because of its negative permeability, the group and phase velocity of the electromagnetic wave are in opposite directions [30]. The occurrence of return loss when the power has been returned to the source is mitigated by the MIA bottom SRR meta-material to reverse the reflected propagation direction and the energy flow of the returned power to radiate efficiently. This phenomenon reduces the reflection coefficient up to -82.95dB and matches the impedance of an antenna.

In Figure 5.4, the 2x1 antenna has a return loss of -60.3 dB and -63.575 dB without

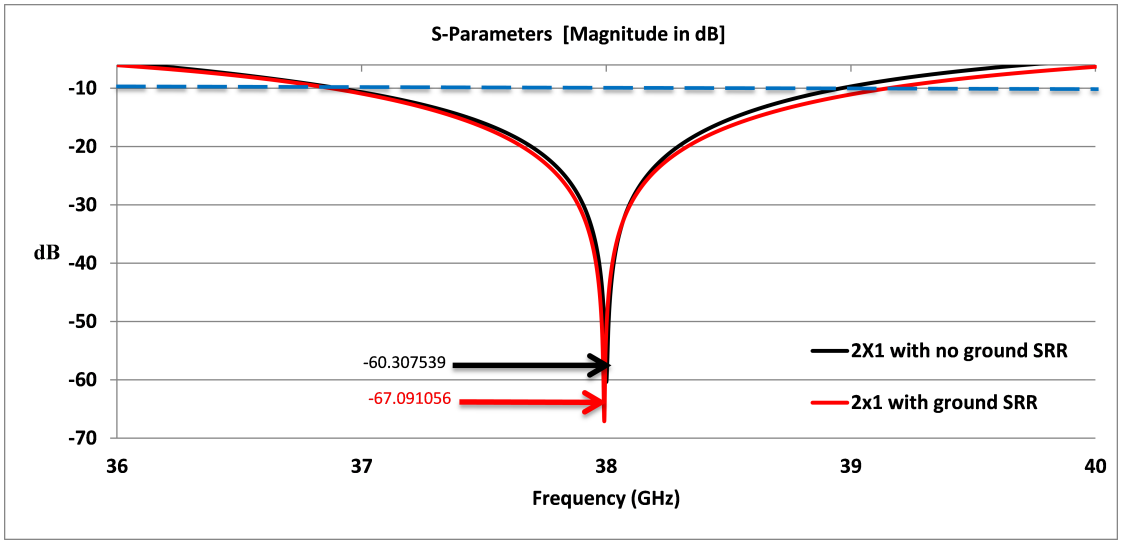

Figure 5.4: Return loss of 2x1 MIA.

SRR array at the ground and 6x4 SRR of array meta-materials at the ground. Here the bandwidth of the 2x1 antenna has been enhanced by using SRR meta-materials from 2.057 GHz to 2.279 GHz. The enhanced bandwidth by using meta-materials is 222 MHz. Also Figure 5.5, it is also clear that the 4 x 1 MIA return losses without

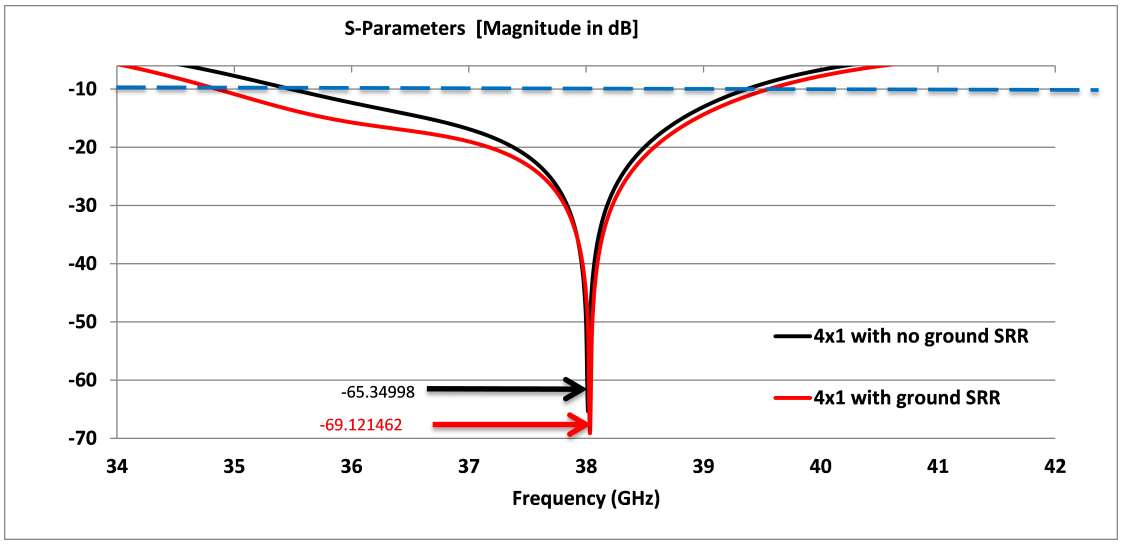

Figure 5.5: The return loss of 4x1 MIA.

and with SRR slots on the ground are -65.35 dB and -69.12 dB, respectively. The antenna's bandwidth was approximately 3.89 GHz before the use of meta-materials, and it increased to 4.704 GHz following the application of meta-materials. As such, it is clear from the results that, by arranging the flow of current to the center of the

patch and decreasing the impedance, the inserted meta-materials at the edge of each MPA attenuate the circulation current which causes a large magnitude of the return losses. As shown in Figure 5.6 the return loss of the 2x2 MIA arrays are -64.75dB and -

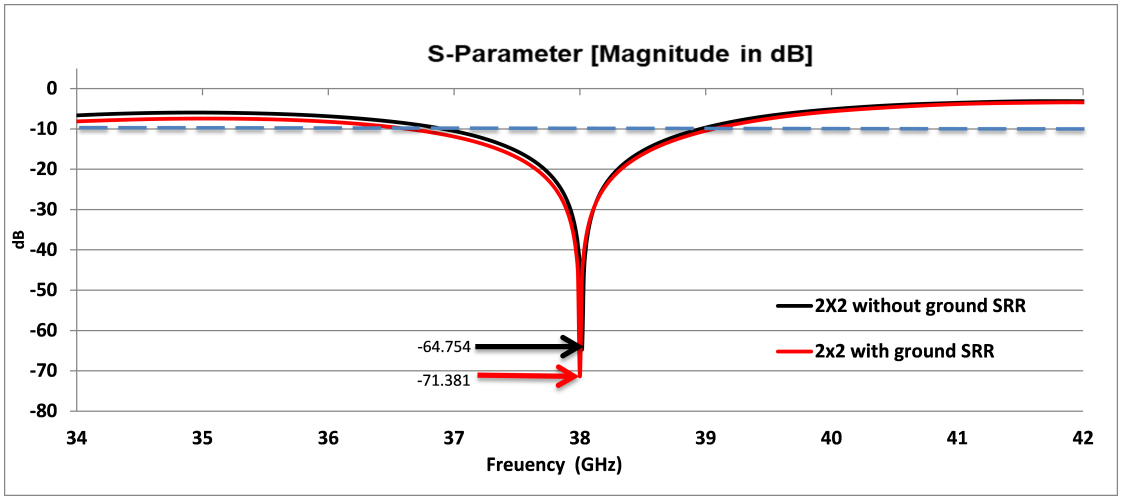

Figure 5.6: The return loss of 2x2 MIA.

71.38dB without and with added ground SRR structure slots. These 2x2 MIA-designed antenna arrays have a bandwidth of 2.043 GHz and 2.43 GHz respectively, which has an improvement of 387MHz. In regards to this result the selected type of ground SRR improves the loss which is accountable as a drawback in conventional antennas. Figure

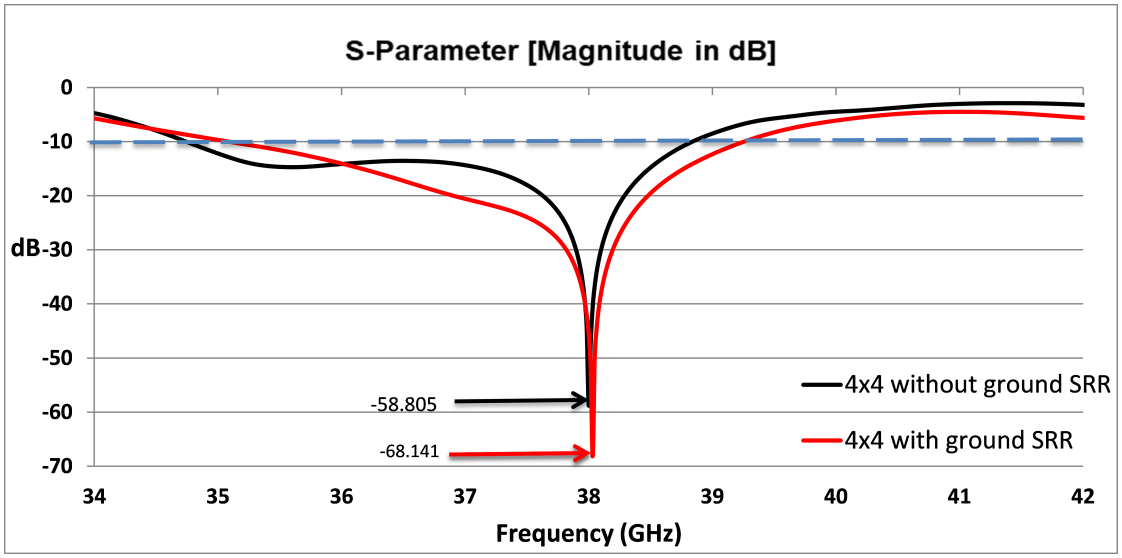

Figure 5.7: The return loss of 4x4 MIA.

5.7 shows the return loss of 4x4 MIA arrays without and with SRR structure slots of its ground. Here the proposed antennas are the added SRR structure slots on the

radiators and the ground respectively. This makes efficient and fully performed design for 5G generations by a return loss result of -58.805dB and -68.14dB, and bandwidths of 4.096GHz and 4.168GHz respectively. The proposed 4x4 MIA antenna design has a bandwidth of 4.168GHz with great performance which is unknown and impossible to design with conventional materials. Figure 5.8 shows the results of 8x8 MIA arrays

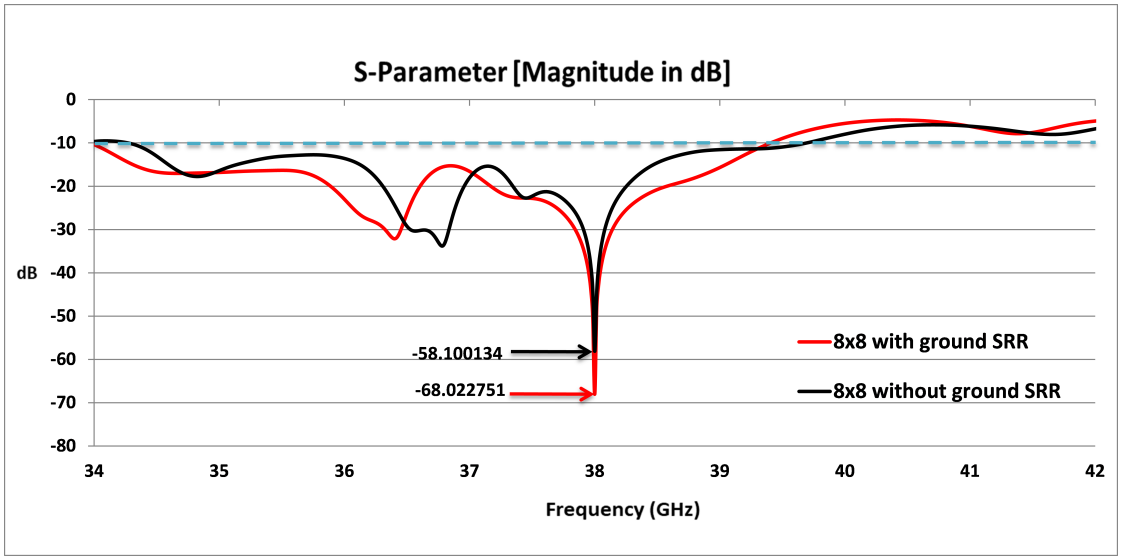

Figure 5.8: The return loss of 8x8 MIA.

return loss for the conventional ground and the final proposed metamaterial-inspired antenna arrays. This paper proposes the newly emerged idea of metamaterial-inspired antenna arrays to fulfill the requirements of 5G technologies. Furthermore, using more matched impedance is the aim of this proposed paper. So, the return loss result of this designed antenna is -58.1dB and -68.023dB of the conventional copper and slotted SRR structure ground respectively. To make enhanced bandwidth 17x17 SRR structure slot has been integrated into the ground of 8x8 MIA arrays. By this method of design, its bandwidth is improved from 5.421 GHz to 5.44 GHz. This enables an additional bandwidth of 19 MHz, with high performance.

The voltage standing wave ratio (VSWR) or standing wave ratio (SWR) is an indication of the amount of mismatch between an antenna and the feed line connecting to the radiator antenna. Additionally, it quantifies the effectiveness of transmitting radio frequency power from a power source, traveling through a feed line, and reaching

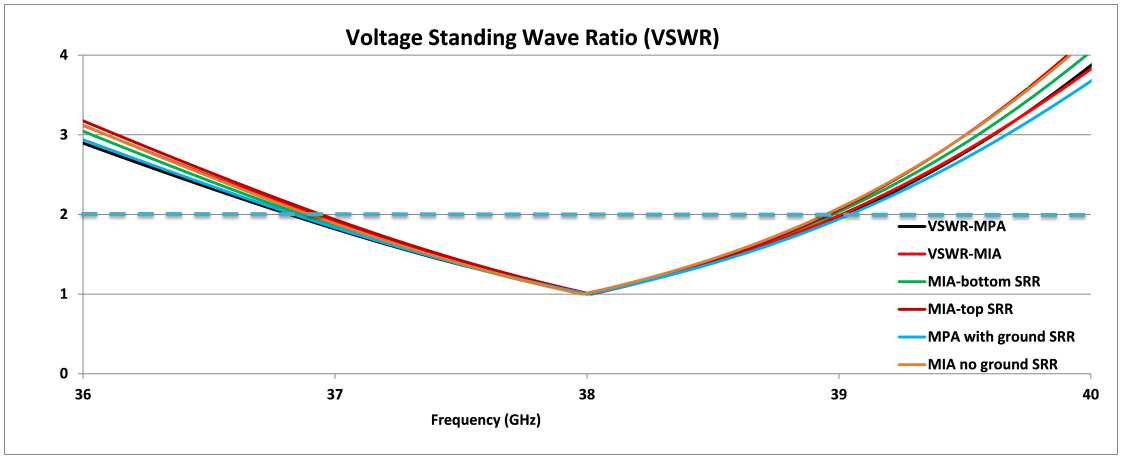

Figure 5.9: VSWR of single MPA and MIA.

a load. In most antenna applications, a VSWR (Voltage Standing Wave Ratio) below 2 is deemed acceptable, with the minimum value at 1.0. The minimum VSWR is 1.0; this means that no power is reflected from the antenna, which is ideal. A good match antenna has a VSWR value that does not exceed 2. Figure 5.9 shows the VSWR result

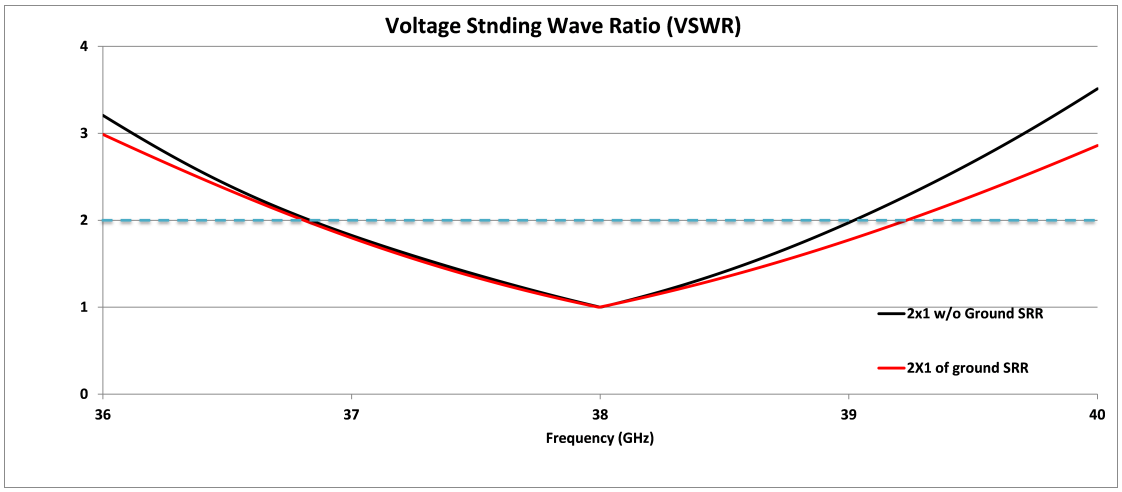

Figure 5.10: VSWR of 2x1 MIA.

of conventional microstrip antenna and the result of single meta-material-inspired antennas for comparison with the studied work respectively. Figure 5.10 was the VSWR result of introduced SRR meta-materials on the antenna of 2x1 meta-material-inspired antenna in the patch and its ground respectively.

Figure 5.11 shows the VSWR of 4 x 1 without SRR slots on the ground of antennas is 1.0002 and with SRR slots 1.0007 respectively. From the results, it can be observed that the introduced metamaterial at the side of the feed line reduces the mismatch loss

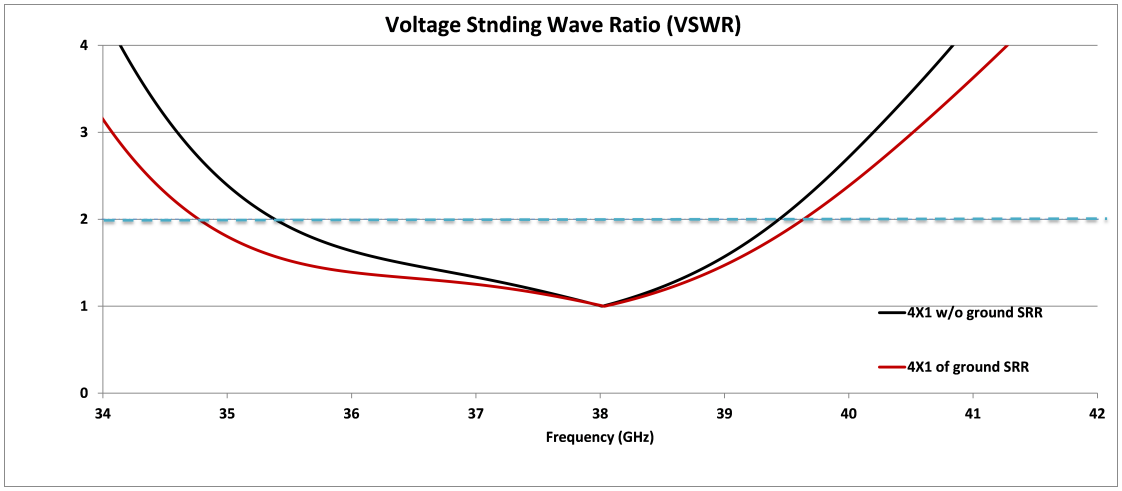

Figure 5.11: VSWR of 4x1 MIA.

of the antenna and can be considered an effective way to minimize the mismatch loss of conventional microstrip antennas. Figure 5.12 shows the 2x2 MIA of a VSWR of

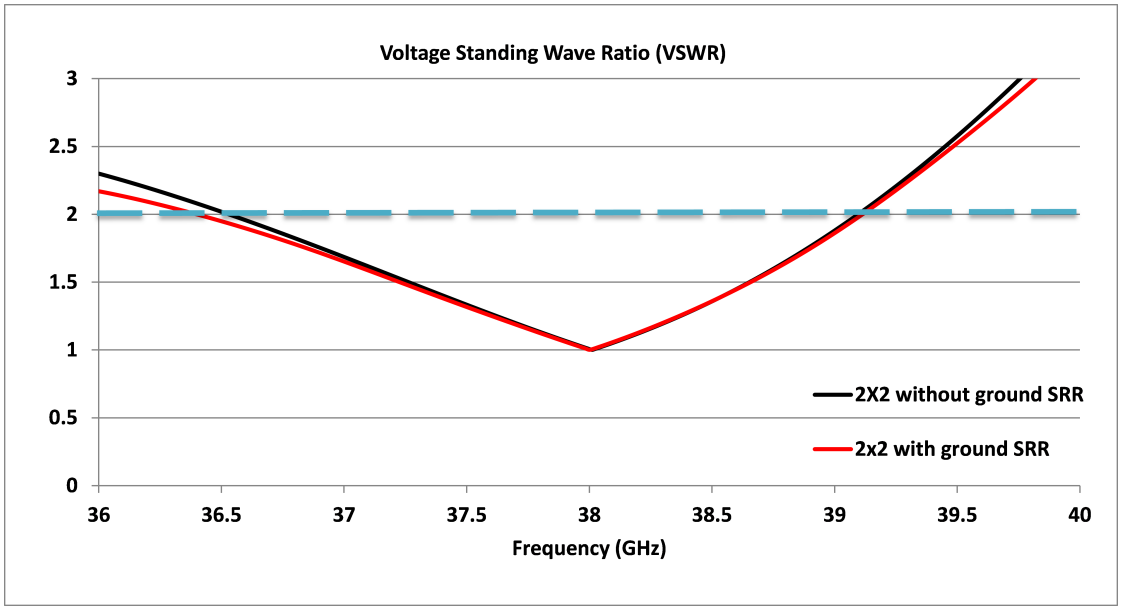

Figure 5.12: VSWR of 2X2 MIA.

1.001158 and 1.00054 for conventional copper and the added SRR structure slots at the radiator's ground. To fulfill the requirements for 5G wireless applications matching an impedance of array antennas is the basic stepping of the design. By considering this scenario the VSWR has approximately ideal antennas. As known in the above Figure 5.13 proposed design the VSWR of 4X4 MIA arrays are highly effective in terms of different papers presented in Table 5.2. The conventional ground of 4x4 MIAs VSWR is

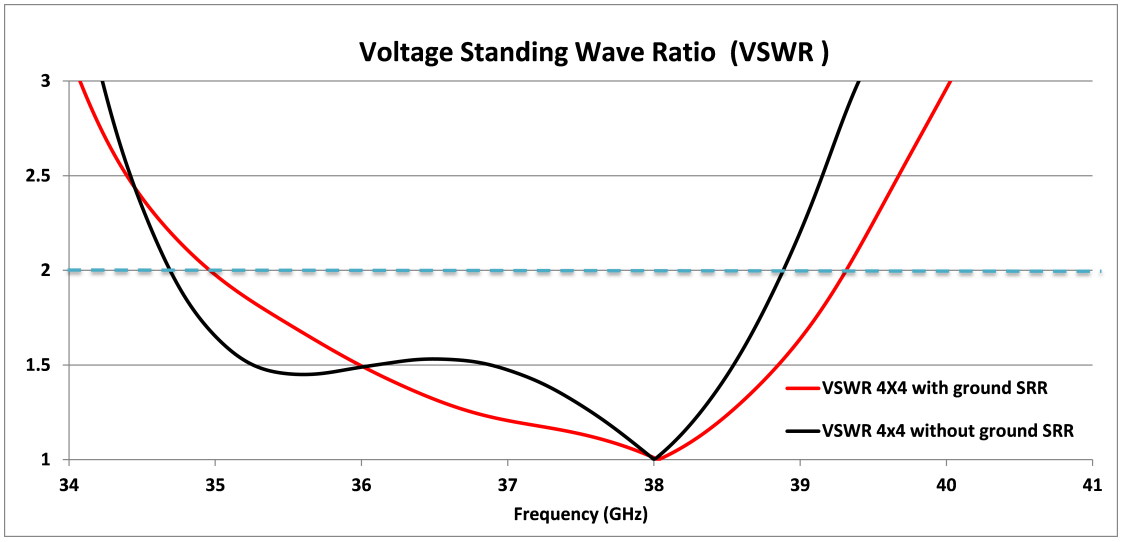

Figure 5.13: VSWR of 4x4 MIA.

1.0023, while the slotted ground is 1.00078. Figure 5.14 VSWR has a VSWR of 1.003

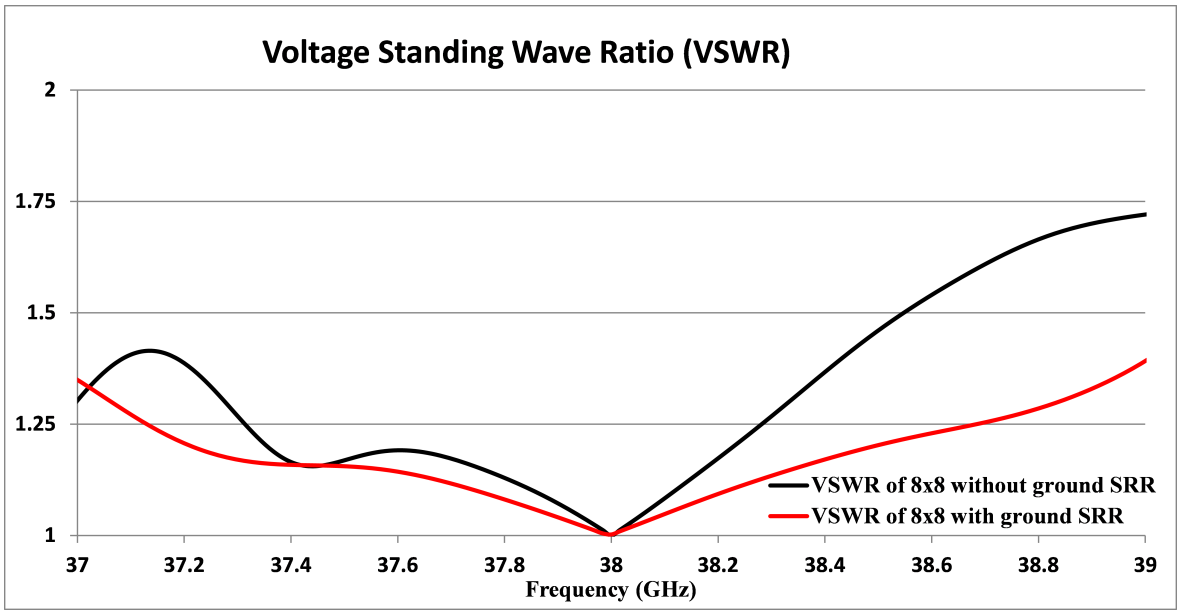

Figure 5.14: VSWR of 8x8 MIA.

and 1.0008 without being added and with SRR structure slots on the 8x8 radiators ground respectively. This enables the designed 8x8 MIA arrays to operate without any mismatch loss and radiate the entire incoming source to the receiver.

The above Figures (i.e. Figure 5.9, 5.10, 5.11, 5.12, 5.13, and 5.14) show the voltage standing wave ratio of single, 2x1, 4x1, 2x2, 4x4, and 8x8 antenna at the center frequency of 38 GHz. A conventional MPA has a VSWR of 1.0181548 and a single

MIA has a value of 1.001432. Therefore, the introduced meta-material at the side of the feed line (bottom SRR) helps us to reduce the mismatch loss of the antenna. As shown in Figures (5.10, 5.11,5.12, 5.13, and 5.14) the VSWR result was 1.0019, 1.0002, 1.001158, 1.0023, and 1.003 for 2x1, 4x1, 2x2, 4x4, and 8x8 without the introduced SRR meta-materials at the ground of antennas and the VSWR of the proposed work (i.e. MIA) for a single, 2x1 4x1, 2x2, 4x4, and 8x8 are 1.001432, 1.0009, 1.0007, 1.00054, 1.00078, and 1.0008 respectively. Therefore to get less mismatching, introducing SRR meta-materials to the antenna is an effective way and the result was approximately related to the ideal VSWR. The mismatched loss was mitigated by the way of this proposed work of MIAs.

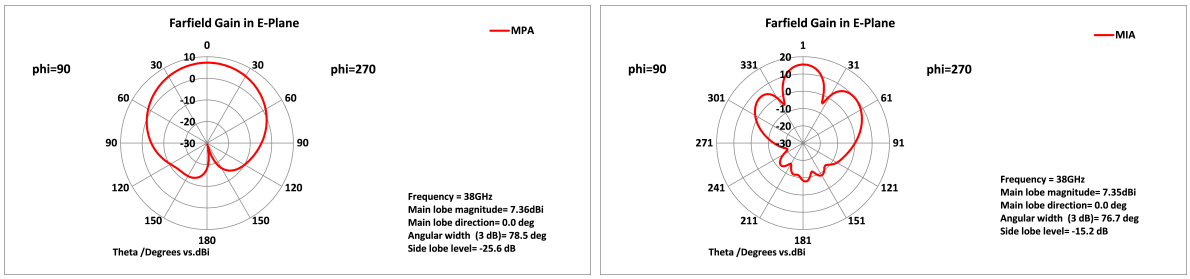

(a) Single MPA. (b) Single MIA antenna.

Figure 5.15: 2D radiation configurations of MPA and MIA antenna in different scenarios.

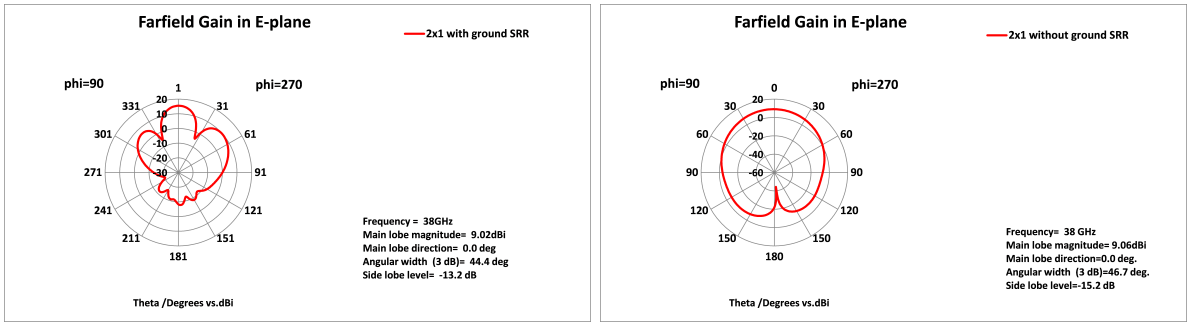

(a) 2x1 MIA without SRR at the ground. (b) 2x1 MIA with 6x4 of SRR at the ground.

Figure 5.16: 2D radiation configuration of 2x1 MIA.

The 2D radiation pattern of a typical 4 x 1 array is given in Figure 5.17(a)-(b). As the SRR slot is introduced only on the radiating patch of the 4x1 array the achieved side lobe level is about -11.3 dB. Likewise, as the SRR slot is integrated on the radiator and ground plane of the array simultaneously, the obtained side lobe level of 4 x 1 MIA

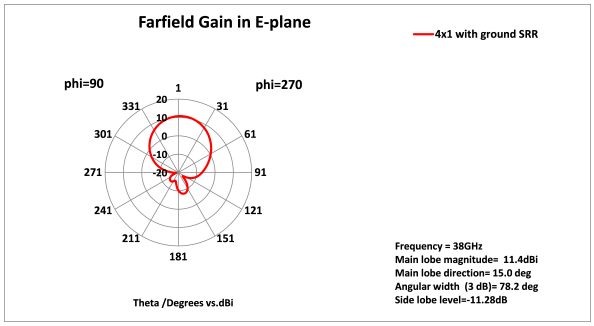

(a) 4x1 MIA without SRR at the ground.

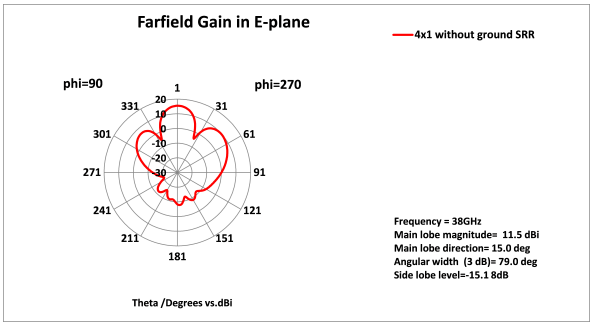

(b) 4x1 MIA with 19x19 of SRR at the ground.

Figure 5.17: 2D radiation configuration of 4x1 MIA.

arrays is -15.2 dB. From the results, it can be easily realized that, as the number of SRR slot arrays on the ground plane increases, the magnitude of the side lobe level increases which is a loss of input power and produces interference at the receiver side. Because the SRR slot arrays reflect the radiated EM in an undesired direction. However, deploying the SRR sots on the ground enhances the bandwidth of all the designed antennas. As shown in Figures 5.15, 5.16, 5.17, 5.18, 5.19 and 5.20 the result

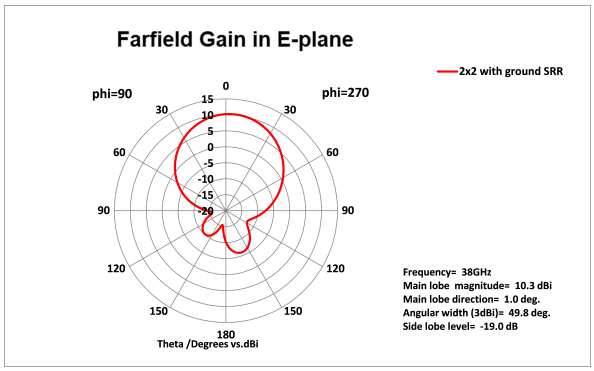

(a) 2x2 MIA without SRR at the ground.

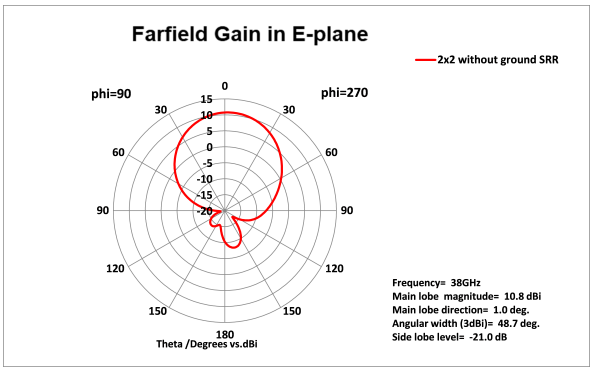

(b) 2x2 MIA with 8x8 of SRR at the ground.

Figure 5.18: 2D radiation configuration of 2x2 MIA.

shows the two-dimensional (2D) result of single, 2x1, 4x1, 2x2, 4x4, and 8x8 MIA. Figure 5.15 are the 2D of a conventional antenna and single MIA with the result side lobe level and angular width of -25.6 dB, 78.5^o and -15.2 dB, 76.3^o respectively. Figure 5.16 are 2x1 MIA without ground SRR of the patch and ground antennas. These show the result of side lobe level and angular width of -15.6 dB, 45.5^o and -13.6 dB, 44.1^o. Figure 5.17 are 4x1 MIA of SRR and with the patch and ground of antennas. These show the result of side lobe level and angular width of -15.6 dB, 45.5^o and -13.6

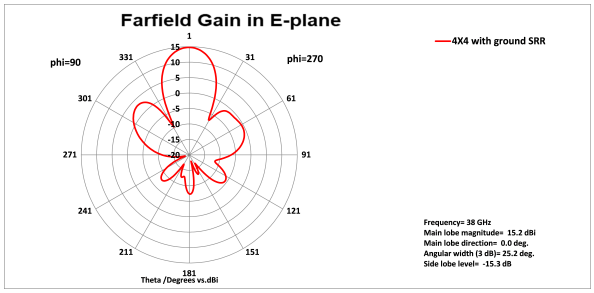

(a) 4x4 MIA without SRR at the ground.

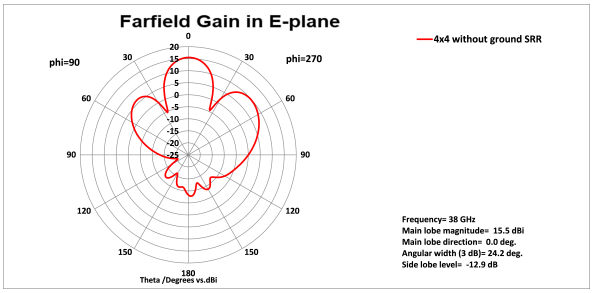

(b) 4x4 MIA with 19x19 of SRR at the ground.

Figure 5.19: 2D radiation configurations of 4x4 MIA.

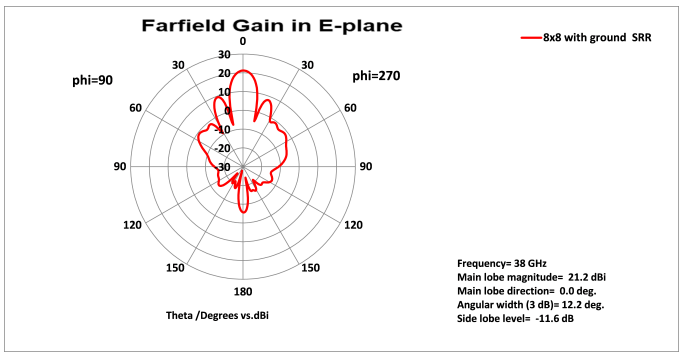

(a) 8x8 MIA without SRR at the ground.

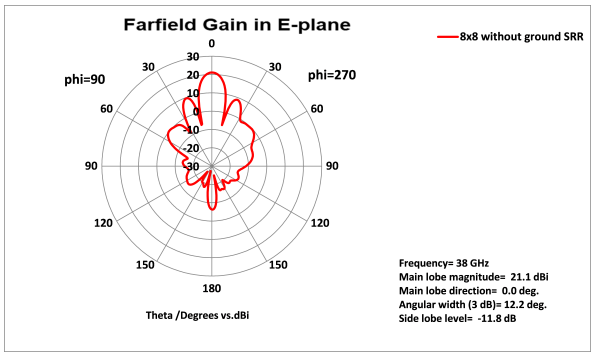

(b) 8x8 MIA with 17x17 of SRR at the ground.

Figure 5.20: 2D radiation configuration of 8x8 MIA.

dB, 44.1^o. Figures 5.18 are 2x2 MIA-inspired meta-material without ground SRR, and with both sides of antennas have the side lobe level and angular width of -21.2 dB, 48.7^o and -19.0 dB, 49.8^o. Figures 5.19 are 4x4 MIA-inspired meta-material with the patch only and with the patch and ground of SRR, has the side lobe level and angular width of -12.8 dB, 24.3^o and -11.6 dB, 24.3 respectively. Figures 5.20 show that the 8x8 MIA of antenna arrays with more performed capacity. In this figure the side lobe level and angular width of -11.8 dB, 12.2^o and -11.6 dB, 12.4^o. All of the proposed work has the main lobe direction at zero degrees and introducing meta-materials with the ground increases the bandwidth of single, 2x1, 4x1, 2x2, 4x4, and 8x8 MIA respectively.

Figure 5.21a shows the gain, radiation efficiency, and total efficiency of a conventional MPA which is 7.24dBi, -0.1261dB, and -0.1264dB (97.13%), and Figure 5.21b is the result of a single MIA is also, 7.36dBi, -0.1978dB, -0.1978dB (95.55%) respectively. Figure 5.22 (a and b) is the result of 2x1 MIA which is inspired by metamaterial in the patch (Figure 5.22a) and introduced SRR metamaterial in the patch and at the ground of the antenna by 6x4 SRR arrays (Figure 5.22b). The gain, radiation

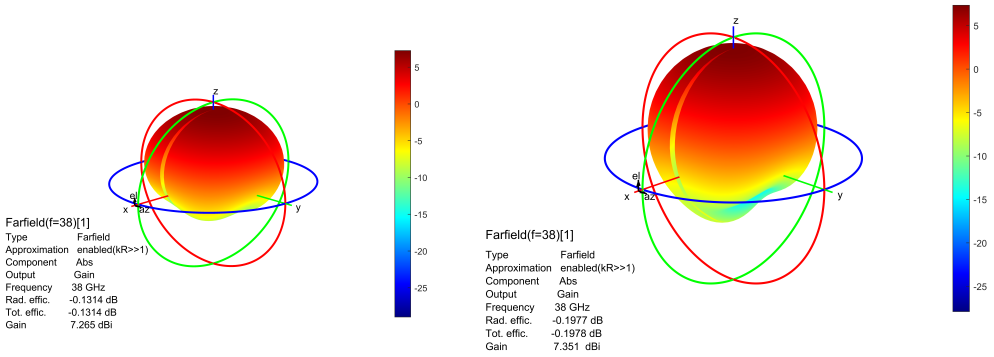

(a) Single MPA. (b) Single MIA antenna.

Figure 5.21: 3D radiation configurations of MPA and MIA antenna in different scenarios.

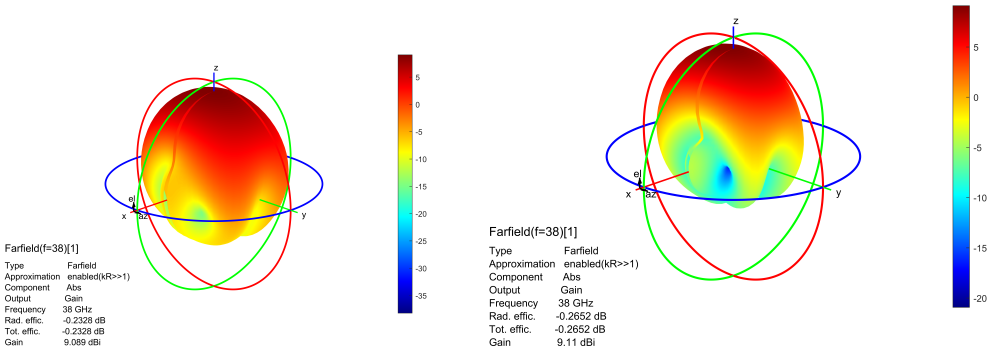

(a) 2x1 MIA with no ground SRR (b) 2x1 MIA array antenna.

Figure 5.22: 3D radiation configuration of 2x1 MIA antenna arrays.

efficiency, and total efficiency are 9.09 dBi, -0.2328dB, and -0.2328dB (94.78%) for Figure 5.22a is 9.11dBi, -0.2652dB, -0.2652dB (94.01%) for Figure5.22b respectively. Figure 5.23 implies that by introducing SRR slots only on the patch and then on both the patch and ground of antennas, the achieved gain, radiation efficiency, and total radiation efficiency of 4 x 1 MIA arrays are about 11.5 dBi, 95.77%, and 11.4 dBi, 95.87%, respectively. Figure 5.24a and b result of 2x2 MIA is 10.8 dBi, -0.2375dB and -0.2375dB (94.68%) introduced metamaterial with the patch only and 11 dBi, -0.1952dB and -0.1962dB (95.58%) introduced metamaterial with patch and ground of antenna respectively. Figure 5.25a and b result of 4x4 MIA is 15.4 dBi, -0.304dB and -0.3042dB (93.23%) introduced metamaterial with the patch only and 14.8 dBi, -0.3101dB and -0.3101dB (93.21%) introduced metamaterial with patch and ground of antenna respectively. Figure 5.26a and b result of 8x8 MIA is 21.23 dBi, -0.5840dB,

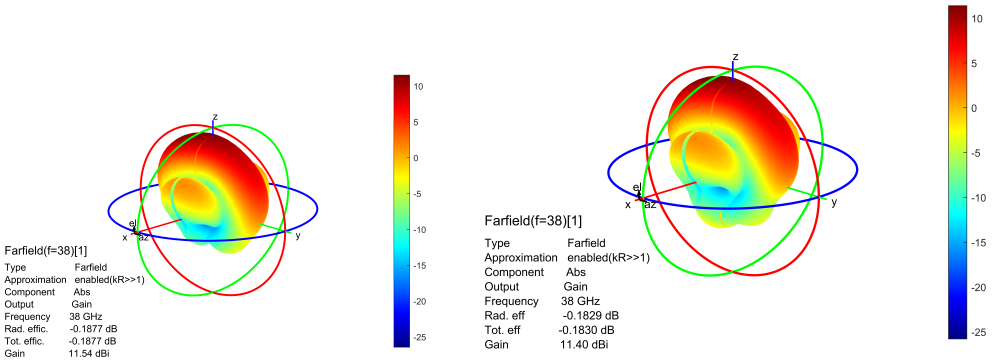

(a) 4x1 MIA with no ground SRR (b) 4x1 MIA array antenna.

Figure 5.23: 3D radiation configuration of 4x1 MIA antenna arrays.

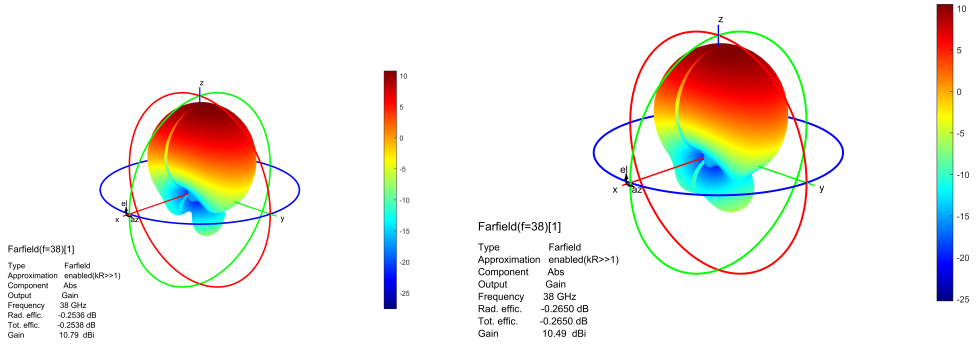

(a) 2x2 MIA with no ground SRR (b) 2x2 MIA array antenna.

Figure 5.24: 3D radiation configuration of 2x2 MIA antenna arrays.

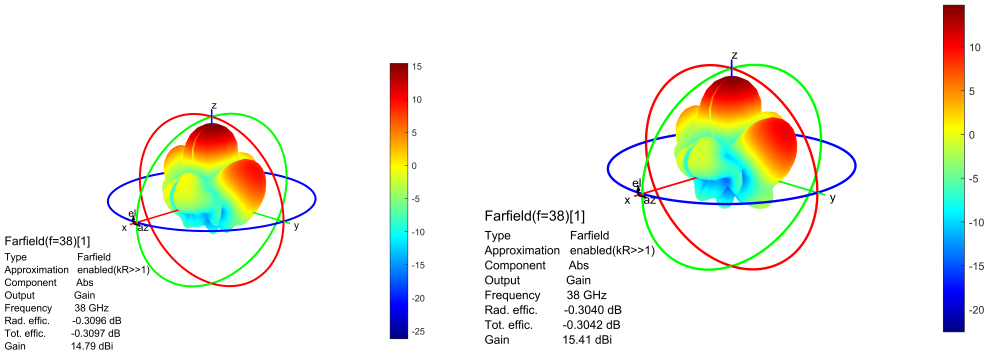

(a) 4x4 MIA with no ground SRR (b) 4x4 MIA with ground of 19x19 SRR .

Figure 5.25: 3D radiation configuration of 4x4 MIA antenna arrays.

and -0.5841dB(87.41%) introduced metamaterial with the patch only and 21.13 dBi, -0.5368dB and -0.6864dB (85.38%) introduced metamaterial with patch and ground of antenna respectively.

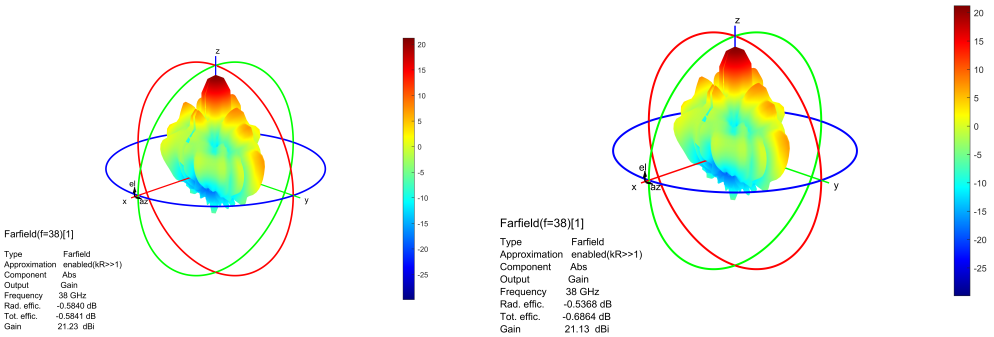

(a) 8x8 MIA with no ground SRR (b) 8x8 MIA with ground of 17x17 SRR .

Figure 5.26: 3D radiation configuration of 8x8 MIA antenna arrays.

Table 5.1: Result of the antenna design performance at 38GHz center frequency.

Antenna parameters	**MPA**	**MIA**	**2x1 MIA**	**4x1 MIA**	**2x2 MIA**	**4x4 MIA**	**8X8 MIA**
Bandwidth (GHz)	2.081	1.971	2.279	4.704	2.51	4.156	5.44
Return loss (dB)	-57.42	-82.95	-67.1	-69.12	-68.81	-68.14	-68.023
VSWR	1.018155	1.001432	1.0009	1.0007	1.00072	1.0078	1.0008
Gain (dBi)	7.24	7.36	9.11	11.4	10.8	14.8	21.13
Directivity (dBi)	7.36	7.55	9.37	11.6	11	15.2	21.67
Radiation efficiency (dB)	-0.1264	-0.1954	-0.2652	-0.1830	-0.1952	-0.3101	-0.5368
Total efficiency (%)	97.13	95.55	94.01	95.87	95.58	93.11	85.38

As shown in table 5.2, the proposed work has high performance compared to existing works. The proposed work of a single metamaterial-inspired antenna has very low return loss, small VSWR, and enhanced efficiency as compared to the reported literature in [32, 33, 36, 38] and the bandwidth also has large when compared to the reported literature in [36, 38]. The array antenna result of 2x1, 4x1, 2x2,4x4, and 8x8 MIA has a better performance than the reported papers in [33, 35] and [31, 37] concerning return loss, VSWR, and total efficiency respectively.

The proposed metamaterial-inspired antenna at the center frequency of 38 GHz will fulfill the requirements of 5G wireless applications rather than the existing works. The

reason for achieving this performance was the sake of using metamaterials on antennas and the ground of antennas. Because of the negative refractive index properties of metamaterials; reduced returned power to the source, increased the fringing effect, and radiation efficiencies of the proposed work have been achieved by metamaterials on antennas. The introduced metamaterials at the ground of the antenna enhance the bandwidth by reducing the surface wave loss and achieving the required performance of 5G wireless applications.

Table 5.2: Comparison of existing works with the result of the proposed work at the center frequency of 38GHz.

Antenna type	**Ref**	**RF(GHz)**	**BW(GHz)**	**S11(dB)**	**VSWR**	**Gain(dBi)**	$\eta(\%)$
Single	[32]	38	2.146	-40.54	1.02	6.85	95.4
	[33]	38	−−	-20.15	1.27	8	90.32
	[36]	38	1.27	-42.78	1.08	9.025	83.61
	[58]	28	0.572	-20.23	1.21	7.18	94.27
	This work	**38**	**1.971**	**-82.95**	**1.001432**	**7.36**	**95.55**
2x1	[33]	38	3.651	-18.35	1.27	9.24	89.63
	[35]	38	1.06	-22.6	−−	9.75	80
	[58]	28	0.575	-19.88	1.34	9.3	92.53
	This work	**38**	**2.279**	**-67.1**	**1.0009**	**9.11**	**94.01**
4x1	[56]	38	3.33	-20.15	1.27	5.5	84
	[57]	38	1.48	-24.25	−−	6.98	−−
	[58]	28	1.394	-27.42	1.106	11.06	96.56
	This work	**38**	**4.704**	**-69.12**	**1.0007**	**11.4**	**95.87**
2x2	[31]	38	3.33	-20.15	1.27	5.5	84
	[37]	38	1.48	-24.25	−−	6.98	−−
	[58]	28	0.326	-32.7	1.05	10.71	89.79
	This work	**38**	**2.51**	**-68.81**	**1.00072**	**10.8**	**95.58**
4x4	[39]	38	3.7	-35	−−	7.49	88
	[44]	38	2	-40.36	−−	5.72	71.35
	[45]	39	1.43	-20	−−	6.4	92
	[58]	28	0.332	-33.15	1.045	15.17	85.08
	This work	**38**	**4.156**	**-68.14**	**1.00078**	**14.8**	**93.21**
8x8	[42]	38	1.294	-15.76	−−	13.4	89.63
	[43]	35	1.162	-40.01	−−	13.728	70.91
	[58]	28	0.368	-17.797	1.3	18.33	74.28
	This work	**38**	**5.44**	**-68.023**	**1.0008**	**21.13**	**85.38**

Chapter 6

6 Conclusions and Recommendations

6.1 Conclusions

MIAs of single, 2x1, 4x1, 2x2, 4x4, and 8x8 antenna array at a center frequency of 38 GHz is designed, simulated, and presented. At first, a single microstrip antenna is designed by the calculated antenna parameters to compare with the designed meta-material-inspired single antennas. The designed MIA has a size of less than the microstrip antenna by 8%. The microstrip antenna and MIA have a bandwidth, return-loss, VSWR, gain, and total efficiency of 2.081GHz, -57.422dB, 1.018155, 7.24dBi and 97.13%; and 1.97GHz, -82.95dB, 1.001432, 7.36dBi and 95.55%; and respectively. Also, 2x1, 4x1, 2x2, 4x4, and 8x8 MIA of bandwidth, return loss, VSWR, gain, and total efficiency has a result 2.279GHz, -63.375dB, 1.001309, 9.11dBi and 94.01%; and 4.704 GHz, -69.12 dB, 1.0007, 11.4 dBi and 95.87%; and 2.51 GHz, -68.81 dB, 1.00072, 10.8 dBi, and 95.58%; and 4.156 GHz, -68.14 dB, 1.00078, 14.8 dBi, and 93.12%; and 5.44 GHz, -68.023 dB, 1.0008, 21.13 dBi, and 85.38% respectively. In this thesis, the bandwidth and radiation efficiency of the 8x8 antenna was 5.44 GHz, and 85.38% respectively. The enhanced performance of this antenna is because of the inspired antennas by meta-materials on the radiators and the ground respectively. This means that as the number of meta-materials increases at the ground of the antenna the surface wave loss decreases and antenna performance will be increased. The suggested antenna's bandwidth expanded and its return loss and VSWR decreased as a result of the antennas' inspiration from meta-materials in the radiator ground and antenna section, respectively.

In this thesis, the simulation and analysis of the proposed work improves the performance and drawbacks of different antennas for 5G wireless applications. To develop the capacities and performances of MIAs, the chosen unit cell metamaterials with modified design were selected and placed with their role and properties.

6.2 Recommendations

This study proves that metamaterial-inspired antenna arrays have fulfilled the requirements of 5G mm-wave wireless technologies. In regards to radiation intensity, VSWR, return loss, gain, beam width, directivity, and efficiencies; this paper achieves the requirements of 5G wireless applications. Especially, to improve fringing effects, size compactness, and reduce the surface and spurious wave losses of the traditional antennas. However, this paper needs more consideration in terms of:

- Analyzing different methods for a gain performance of metamaterial-inspired antenna arrays to enhance and increase as the metamaterial slots have emerged to different proposed antennas.
- Studying the simulation difficulties of antenna arrays when more slots of metamaterials are added to inspire and motivate antenna performances.
- Analyzing the performances of metamaterial-inspired antenna arrays as the resonance frequency is operated at multi-band frequencies. As different frequencies are operated at the same antennas, more mutual coupling and cross-polarization appear which degrades an antenna's performance.

References

[1] Hemadeh, Ibrahim A., Katla Satyanarayana, Mohammed El-Hajjar, and Lajos Hanzo. "Millimeter-wave communications: Physical channel models, design considerations, antenna constructions, and link-budget." IEEE Communications Surveys and Tutorials 20, no. 2 (2017): 870-913.

[2] Rappaport, Theodore S., Robert W. Heath Jr, Robert C. Daniels, and James N. Murdock. Millimeter wave wireless communications. Pearson Education, 2015.

[3] Dahlman, Erik, Stefan Parkvall, and Johan Skold. 5G NR: The next generation wireless access technology. Academic Press, 2020.

[4] Manuel Garc´ıa Sanchez, "Millimeter-wave communication." Printed Edition of the Special Issue Published in Electronics, ISSN 2079-9292, 2020.

[5] Walser RM. Electromagnetic metamaterials. In Proc: SPIE 4467 Complex Mediums II: Beyond Linear Isotropic Dielectrics, San Diego, CA, USA; 2001. pp. 1-15.

[6] Caloz C, Itoh T. Application of the transmission line theory of left-handed (LH) materials to the realization of a microstrip LH line. In: Proceedings of the IEEE Antennas and Propagation Society International Symposium. 2002. pp. 412-415. DOI: 10.1109/APS.2002.1016111.

[7] Zheludev NI, Kivshar YS. From metamaterials to metadevices. Nature Materials. 2012;11: 917-924. DOI: 10.1038/nmat3431.

[8] Yayun D, Wenwen L, Xijun Y, Chen Y, Houjun T. Design of unit cell for metamaterials applied in a wireless power transfer system. In: IEEE Pels Workshop on Emerging Technologies: Wireless Power Transfer. 2017. pp. 143-147. DOI: 10.1109/WoW.2017.7959382.

[9] zhan DT, Phan HL, Nguyen TQH. A miniaturization of microstrip antenna using negative permittivity metamaterial based on CSRR loaded ground for WLAN applications. Journal of Science and Technology. 2016;54(6):689-697. DOI: 10.15625/0866-708X/54/6/8375.

[10] Ramachandran, T., Faruque, M.R.I. and Islam, M.T. Specific absorption rate reduction for sub-6 frequency range using polarization dependent metamaterial with high effective medium ratio. Sci Rep 12, 1803 (2022). doi.org/10.1038/s41598-022-05851-2

[11] Abubar, Abd Rahman, Mutiara Widasari Sitopu, Panangian Mahadi Sihombing, Jhoni Hidayat, and Afandi Sahputra. "Microstrip Antenna Design with Left Handed Metamaterial (LHM) for Automatic Dependent Surveillance-Broadcast (ADS-B)." In 2020 4th International Conference on Electrical, Telecommunication and Computer Engineering (ELTICOM), pp. 103- 106. IEEE, 2020.

[12] Pattar, Deepa, Preeti Dongaokar, and S. L. Nisha. "Metamaterial for design of Compact Microstrip Patch Antenna." In 2020 IEEE Bangalore Humanitarian Technology Conference (B-HTC), pp. 1-4. IEEE, 2020.

[13] Reena, Parihar. "A Compact Metamaterial inspired Dual-band SRR loaded Antenna for Wireless Applications." Research Journal of Quantum Computations and Physical Systems Vol 1 (2018): 1.

[14] Islam, Afia Mubassira, Emraul Islam Emon, and Anis Ahmed. "A Metamaterial Loaded Microstrip Patch Antenna for Lower 5G U-NII Spectrum A Metamaterial Loaded Microstrip Patch Antenna for Lower 5G U-NII Spectrum."

[15] Smari, Bouthaina, Mondher Labidi, and Fethi choubani. "Mutual coupling reduction in metamaterial antenna for terahertz application." Applied Physics A 125 (2019): 1-7.

[16] Baena, J. D., A. C. Escobar, A. Sayanskiy, and S. B. Glybovski. "Lefthanded metamaterials matched to free space through mechanical tuning." In 2019 Thirteenth international congress on artificial materials for novel wave phenomena (Metamaterials), pp. X-044. IEEE, 2019.

[17] Baena, J. D., A. C. Escobar, A. Sayanskiy, and S. B. Glybovski. "Lefthanded metamaterials matched to free space through mechanical tuning." In 2019 Thirteenth

international congress on artificial materials for novel wave phenomena (Metamaterials), pp. X-044. IEEE, 2019.

[18] Jairath, Kapil, Navdeep Singh, Vishal Jagota, and Mohammad Shabaz. "Compact ultrawide band metamaterial-inspired split ring resonator structure loaded band notched antenna." Mathematical Problems in Engineering 2021 (2021).

[19] Kaushal, Akshta, and Gaurav Bharadwaj. "Designing of Square Microstrip Patch Antenna using Metamaterial Structure." 2019.

[20] Ki Hamaad, Ehab, and Mohamed Zm Hamdalla.ZM. "Design of miniaturized and high isolation metamaterial-based MIMO antenna for mobile terminals." JES. Journal of Engineering Sciences 45, no. 6 (2017): 763-772.

[21] Archana Mongia, Deepak Vats, "Metamaterial Based Microstrip Patch Antenna Using Unit Cell Array for Gain Enhancement",Journal of Emerging Technologies and Innovative Research (JETIR), June 2019, Volume 6, Issue 6.

[22] Grimberg R. Electromagnetic metamaterials. Materials Science and Engineering B. 2013; 178:1285-1295. DOI: 10.1016/j.mseb.2013.03.022.

[23] Esmail, B. A. F., H. A. Majid, F. A. Saparudin, M. Jusoh, A. Y. Ashyap, Najib Al-Fadhali, and M. K. A. Rahim. "Negative refraction metamaterial with low loss property at millimeter wave spectrum." Bulletin of Electrical Engineering and Informatics 9, no. 3 (2020): 1038-1045.

[24] El-Nady, Shaza, Hany Mahmoud Zamel, Moataza Hendy, Abdelhalim A. Zekry, and Ahmed Attiya. "Gain enhancement of a millimeter wave antipodal vivaldi antenna by epsilon-near-zero metamaterial." Progress In Electromagnetics Research C 85 (2018): 105-116.

[25] Pourgholamhossein, Zohre, and Tayeb A. Denidni. "Wideband Ultrathin Huygens' Metasurface element for 5G Millimeter-Wave Applications." In 2020 IEEE International Symposium on Antennas and Propagation and North American Radio Science Meeting, pp. 453-454. IEEE, 2020.

[26] C. A. Balanis, "Antenna Theory Analysis and Design", John Wiley and Sons Inc.publication,4th Edition, Hoboken, New Jersey: 2010.63

[27] D. M. Pozar, "Microwave Engineering," John Wiley and Sons Inc, 4thedition, 2012,

[28] Alexander Kuchar, "Aperture Coupled Microstrip Patch Antenna Array", March 15, 1996.

[29] Labidi, Mondher, and Fethi Choubani. "A Design of Metamaterials MIMO Antenna for Millimeter Wave Application." In 2019 International Conference on Software, Telecommunications and Computer Networks (SoftCOM), pp. 1-4. IEEE, 2019.

[30] Afia Mubassira Islam*, Emraul Islam Emon, Anis Ahmed, A Metamaterial Loaded Microstrip Patch Antenna for Lower 5G U-NII Spectrum, Department of Electrical and Electronic Engineering, University of Dhaka, Dhaka 1000, Bangladesh.

[31] Rafique, Umair, Shobit Agarwal, Hisham Khalil Nasir Nauman, and Khalil Ullah. "Inset-fed planar antenna array for dual-band 5G MIMO applications." Progress In Electromagnetics Research C 112 (2021): 83-98.

[32] Anas Abu Bakr Binshitwan, Seraj Mohamed keskeso, Abdulmunem Adel Alquzayzi "38GHz Rectangular Microstrip Antenna with DGS for 5G Applications."

[33] Hala Mohammed Marzouk and Abdelhamed Shaalan and Mohamed Ismail Ahmed "A two-element microstrip antenna 28/38 GHz for 5G mobileapplications" Delta University Scientific Journal Volume 3 Issue 1 April (2020).

[34] Mohammad Lutful Hakim, Mohammed Jashim Uddin and MD Jiabul Hoque, "28/38 GHz Dual Band Microstrip Antenna with DGS and Stub-slot Configurations and Its 2x2 MIMO Antenna Design for 5G Wireless Communication."

[35] Mohamad Aizwan Bin, Sulaim Bin Ab Qais, "Design of a Rectangular patch Microstrip Patch Antenna for 5G Applications." University of Technology of Marash Alam Malaysia.

[36] Brajaruta Chauhan, Sandip Vijam and S.C.Gupta. “Millimeter wave mobile communication Microstrip Antenna for 5G –A Future Antenna.” International Journal of Computer Applications, Volume-99-no-19-August 2014.

[37] Samarth Agarwal and Prahi. “High Gain Linear 1x4 X-slotted Microstrip Patch Antenna Array for 5G Mobile Technology.” Model Institute of Engineering and Technology, Jammu, India (2020).

[38] Hassan, Esraa I., Radwa I. Hamad, and Mohamed I. Omar. "A 38 GHz Modified Circular Microstrip Patch Antenna for 5G Mobile Systems." In 2021 38th National Radio Science Conference (NRSC), vol. 1, pp. 56-63. IEEE, 2021.Sabek, Ayman R., Ahmed A. Ibrahim, and Wael A. Ali. "Dual-band millimeter wave microstrip patch antenna with stubresonators for 28/38 GHz applications." In Journal of Physics: Conference Series, vol. 2128, no. 1, p. 012006. IOP Publishing, 2021.

[39] Shehata, Rania Eid A., Ayman Elboushi, Moataza Hindy, and Hamdi Elmekati. "Metamaterial inspired LPDA MIMO array for upper band 5G applications." International Journal of RF and Microwave Computer-Aided Engineering (2022): e23212.

[40] Sajin, Gheorghe Ioan, and Iulia Andreea Mocanu. "Metamaterial CRLH antennas on silicon substrate for millimeter-wave integrated circuits." International Journal of Antennas and Propagation 2012 (2012).

[41] (https://www.geeksforgeeks.org/snells-law-formula/)

[42] Thenmozhi, K., K. Jagadeeshvelan, M. GaneshMadhan, S. Piramasubramanian, and J. Roopchand. "Simulation of microstrip array antenna for ka-band applications." In 2014 International Conference on Electronics and Communication Systems (ICECS), pp. 1-5. IEEE, 2014.

[43] Rahayu, Yusnita, Muhammad Rifqy Asrul, and Tulus Rahayu. "Design MIMO 1x8 Antenna for Future 5G Applications." TELKOMNIKA (Telecommunication Computing Electronics and Control) 16, no. 2 (2018): 600-605.

[44] Tu, Duong Thi Thanh, Nguyen Gia Thang, Nguyen Tuan Ngoc, Nguyen Thi Bich Phuong, and Vu Van Yem. "28/38 GHz dual-band MIMO antenna with low

mutual coupling using novel round patch EBG cell for 5G applications." In 2017 International Conference on Advanced Technologies for Communications (ATC), pp. 64-69. IEEE, 2017.

[45] Rashad, Noha M., Aziza I. Hussein, and Ashraf AM Khalaf. "Two-Element Pharaonic Ankh-Key Array Antenna Design, Simulation, and Fabrication for 5G and Millimeter-Wave Broadband Applications." IEEE Access 10 (2022): 15175-15182.

[46] Buriak, Iryna A., V. O. Zhurba, G. S. Vorobjov, V. R. Kulizhko, O. K. Kononov, and Oleksandr Rybalko. "Metamaterials: Theory, classification and application strategies."

[47] Limaye, A. (2006). Size Reduction of Microstrip Antennas Using Left-Handed Materials Realized by Complementary Split-Ring Resonators. Thesis, Rochester Institute of Technology.

[48] Devarapalli, Ananda Babu, and Tamasi Moyra. "Design of a metamaterial loaded W-shaped patch antenna with FSS for improved bandwidth and gain." Silicon 15, no. 4 (2023): 2011-2024.

[49] Smith, David R., Jonah Gollub, Jack J. Mock, Willie J. Padilla, and David Schurig. "Calculation and measurement of bianisotropy in a split ring resonator metamaterial." Journal of Applied Physics 100, no. 2 (2006).]

[50] Moser, H. O., B. D. F. Casse, O. Wilhelmi, and B. T. Saw. "Electromagnetic metamaterials over the whole THz range–achievements and perspectives." Electromagnetic Materials (2005): 18-25.

[51] Ren, Kun, Pengwen Zhu, Taotao Sun, Junchao Wang, Dawei Wang, Jun Liu, and Wensheng Zhao. 2022. "A Complementary Split-Ring Resonator (CSRR)-Based 2D Displacement Sensor" Symmetry 14, no. 6: 1116. https://doi.org/10.3390/sym14061116.

[52] Li, Aobo, Shreya Singh, and Dan Sievenpiper. "Metasurfaces and their applications." Nanophotonics 7, no. 6 (2018): 989-1011.

[53] Yang, Li, Mingyan Fan, Fanglu Chen, Jingzhao She, and Zhenghe Feng. "A novel compact electromagnetic-bandgap (EBG) structure and its applications for microwave circuits." IEEE Transactions on Microwave Theory and Techniques 53, no. 1 (2005): 183-190.

[54] Daniel F. Sievenpiper and Lijun Zhang and Romulo J. Broas and N. g. Alexopolous and Eli Yablonovitch, "High-impedance electromagnetic surfaces with a forbidden frequency band." IEEE Transactions on Microwave Theory and Techniques, no.47 (1999): 2059-2074.

[55] Anwar, Rana Sadaf, Lingfeng Mao, and Huansheng Ning. "Frequency selective surfaces: A review." Applied Sciences 8, no. 9 (2018): 1689.

[56] Rafique, Umair, Shobit Agarwal, Hisham Khalil Nasir Nauman, and Khalil Ullah. "Inset-fed planar antenna array for dual-band 5G MIMO applications."Progress In Electromagnetics Research C 112, pp. 83-98, 2021.

[57] Samarth Agarwal and Prahi. "High Gain Linear 1x4 X-slotted Microstrip Patch Antenna Array for 5G Mobile Technology."Model Institute of Engineering and Technology, Jammu, India, 2020.

[58] Gemeda, Mulugeta T., and Kinde A. Fante. "Inset-Feed Rectangular Microstrip Patch Antenna Array Performance Enhancement for 5G Mobile Applications."In International Conference on Advances of Science and Technology, pp. 284-303. Springer, Cham, 2020.

7 Appendix

Table 7.1: Bottom and Top SRR Single MIA

Parameters	**Symbol**	**Top SRR(mm)**	**Bottom SRR (mm)**
Ground-plane width	W	5.22	5.22
Ground-plane length	L	4.54	4.54
Patch width	W_{pw}	2.86	2.68
Patch length	L_{pl}	2.36	2.36
Inset feed gap	I_l	0.42	0.42
Inset feed length	I_w	0.17	0.17
Width of feed point	L_{fdp}	1.1323	
Length of feed point	W_{fdp}	1.3985	
Width of feeder line	W_{fline}	0.2	0.2
Length of feeder line	L_{fline}	0.92	0.95
SRR Radiators	SRR	4 Unit Cells	4 Unit Cells
SRR grounds	SRR	No Unit Cells	No Unit Cells

Table 7.2: Dimensions of 2x1 MIA Arrays

Parameters	**Symbol**	**2x1 w/o SRR (mm)**	**2x1 with SRR (mm)**
Ground-plane width	W	8	8
Ground-plane length	L	4.54	4.54
Patch width	W_{pw2x1}	2.23	2.27
Patch length	L_{pl2x1}	2.43	2.39
Inset feed gap	I_{l2x1}	0.4	0.4
Inset feed length	I_{w2x1}	0.15	0.15
Width of feed point	L_{fdp2x1}	1.1323	1.22
Length of feed point	W_{fdp2x1}	1.3985	1.5
Width of feeder line	$W_{fline2x1}$	1.33	1.21
Length of feeder line	$L_{fline2x1}$	0.92	0.92
Length of Power Divider	P_l	3.9	3.9
width of Power Divider	P_d	0.1	0.1
SRR Radiators	SRR	8	8
SRR grounds	SRR	No Unit Cells	24 Unit Cells

Table 7.3: Dimensions of 4x1 MIA Arrays

Parameters	**Symbol**	**4x1 w/o SRR (mm)**	**4x1 with SRR (mm)**
Ground-plane width	W	17	17
Ground-plane length	L	7.5	7.5
Patch width	W_{pw4x1}	2.86	2.69
Patch length	L_{pl4x1}	2.34	2.3
Inset feed gap	I_{l4x1}	0.4	0.4
Inset feed length	I_{w4x1}	0.15	0.15
Width of feed point	L_{fdp4x1}	1.214	1.2
Length of feed point	W_{fdp4x1}	1.3	1.4
Width of feeder line	$W_{fline4x1}$	0.2	0.2
Length of feeder line	$L_{fline4x1}$	1.4	1.4
Length of Power Divider	Pl_{2x1}	3.8	3.8
width of Power Divider	Pd_{2x1}	0.1	0.1
Length of Power Divider	Pl_{2x2}	8	8
width of Power Divider	Pd_{2x2}	0.1	0.1
SRR Radiators	SRR	16 Unit Cells	16 Unit Cells
SRR grounds	SRR	No Unit Cells	112 Unit Cells

Table 7.4: Dimensions of 2x2 MIA Arrays

Parameters	**Symbol**	**2x2 w/o SRR (mm)**	**2x2 with SRR (mm)**
Ground-plane width	W	8	8
Ground-plane length	L	8	8
Patch width	W_{pw2x2}	2.83	2.8
Patch length	L_{pl2x2}	2.47	2.44
Inset feed gap	I_{l2x2}	0.4	0.4
Inset feed length	I_{w2x2}	0.15	0.15
Width of feed point	L_{fdp2x2}	1.1323	1.22
Length of feed point	W_{fdp2x2}	1.3985	1.5
Width of feeder line	$W_{fline2x2}$	1.33	1.21
Length of feeder line	$L_{fline2x2}$	3.6	3.6
Length of Divider 2x1	Pl_{2x1}	4.1	3.9
width of Divider 2x1	Pw_{2x1}	0.1	0.1
Length of Divider 2x2	Pl_{2x2}	3.93	3.93
width of Divider 2x2	Pw_{2x2}	0.1	0.1
SRR Radiators	SRR	16 Unit Cells	16 Unit Cells
SRR grounds	SRR	No Unit Cells	64 Unit Cells

Table 7.5: Dimensions of 4x4 MIA Arrays

Parameters	**Symbol**	**4x4 w/o SRR (mm)**	**4x4 with SRR (mm)**
Ground-plane width	W	20	20
Ground-plane length	L	20	20
Patch width	W_{pw4x4}	2.9	2.84
Patch length	L_{pl4x4}	2.46	2.43
Inset feed gap	I_{l4x4}	0.4	0.4
Inset feed length	I_{w4x4}	0.15	0.15
Width of feed point	L_{fdp4x4}	1.12	1.43
Length of feed point	W_{fdp4x4}	1.52	1.53
Width of feeder line	$W_{fline4x4}$	0.2	0.2
Length of feeder line	$L_{fline4x4}$	9.97	9.95
Length of Divider 2x1	Pl_{2x1}	3.8	3.8
width of Divider 2x1	Pw_{2x1}	0.1	0.1
Length of Divider 2x2	Pl_{2x2}	3.9	3.9
width of Divider 2x2	Pw_{2x2}	0.1	0.1
Length of Divider 4x2	Pl_{4x2}	7.4	7.4
width of Divider 4x2	Pw_{4x2}	0.1	0.1
Length of Divider 8x2	Pl_{8x2}	8.9	8.9
width of Divider 8x2	Pw_{8x2}	0.1	0.1
SRR Radiators	SRR	64 Unit Cells	64 Unit Cells
SRR grounds	SRR	No Unit Cells	361 Unit Cells

Table 7.6: Dimensions of 8x8 MIA Arrays

Parameters	**Symbol**	**8x8 w/o SRR (mm)**	**8x8 with SRR (mm)**
Ground-plane width	W	37	37
Ground-plane length	L	37	37
Patch width	W_{pw8x8}	2.27	2.26
Patch length	L_{pl8x8}	2.42	2.26
Inset feed gap	I_{l8x8}	0.4	0.4
Inset feed length	I_{w8x8}	0.15	0.15
Width of feed point	L_{fdp8x8}	2.3	2
Length of feed point	W_{fdp8x8}	2.2	2
Width of feeder line	$W_{fline8x8}$	0.1	0.1
Length of feeder line	$L_{fline8x8}$	19.98	19.98
Length of Divider 2x1	Pl_{2x1}	3.8	3.8
width of Divider 2x1	Pw_{2x1}	0.2	0.2
Length of Divider 2x2	Pl_{2x2}	3.89	3.8
width of Divider 2x2	Pw_{2x2}	0.1	0.1
Length of Divider 4x2	Pl_{4x2}	7.28	7.2
width of Divider 4x2	Pw_{4x2}	0.1	0.1
Length of Divider 8x2	Pl_{8x2}	7.91	7.91
width of Divider 8x2	Pw_{8x2}	0.1	0.1
Length of Divider 16x2	Pl_{16x2}	15.95	15.95
width of Divider 16x2	Pw_{16x2}	0.1	0.1
Length of Divider 32x2	Pl_{32x2}	15.95	15.95
width of Divider 32x2	Pw_{32x2}	0.2	0.2
SRR Radiators	SRR	256 Unit Cells	256 Unit Cells
SRR grounds	SRR	No Unit Cells	269 Unit Cells